TRANSPORTATION RESEARCH RECORD
581

Innovations in Subsurface Exploration of Soils

5 reports presented at a symposium at the 54th Annual Meeting of the Transportation Research Board

TRB
TRANSPORTATION RESEARCH BOARD
NATIONAL RESEARCH COUNCIL
Washington, D. C., 1976

Transportation Research Record 581
Price $2.40
Edited for TRB by Marianne Cox Wilburn

Subject areas
03 rail transport
21 photogrammetry
35 mineral aggregates
61 exploration-classification (soils)
63 mechanics (earth mass)

The project that is the subject of this report was approved by the Governing Board of the National Research Council, whose members are drawn from the councils of the National Academy of Sciences, the National Academy of Engineering, and the Institute of Medicine. The members of the committee responsible for the report were chosen for their special competence and with regard for appropriate balance.

This report has been reviewed by a group other than the authors according to procedures approved by a Report Review Committee consisting of members of the National Academy of Sciences, the National Academy of Engineering, and the Institute of Medicine.

LIBRARY OF CONGRESS CATALOGING IN PUBLICATION DATA

National Research Council. Transportation Research Board.
Innovations in subsurface exploration of soils.

(Transportation research record; 581)
1. Soil mechanics—Congresses. 2. Prospecting—Geophysical methods—Congresses. I. Title.
II. Series.
TE7.H5 no. 581 [TA710.A1] 380.5'08s [625.7'32]
ISBN 0-309-02495-1 76-40979

CONTENTS

E-PHASE SYSTEM FOR DETECTING BURIED GRANULAR DEPOSITS

R. W. Culley, Saskatchewan Department of Highways and Transportation;
F. L. Jagodits, Barringer Research Ltd., Rexdale, Ontario; and
R. S. Middleton,* Rosario Resources Corp., Toronto, Ontario

In 1968, the Saskatchewan Department of Highways and Transportation began an investigation of airborne geophysical survey methods for mapping buried deposits. Single-frequency E-Phase airborne resistivity surveys were carried out in 1970 and 1971, and multifrequency survey programs began in 1973. The E-Phase airborne resistivity system uses radio wave transmissions to provide the primary field, and it measures the apparent resistivity of the ground at 3 frequencies simultaneously. The measurement of apparent resistivity at 3 frequencies provides information about the subsurface to 3 depths. The correlation between earth materials and resistivities may vary from area to area, but definite limits of resistivity can be assigned for broad ranges of soil classification. The E-Phase survey in the Wadena area of Saskatchewan, where intertill gravel deposits were suspected to exist, resulted in 27 anomalies worthy of follow-up. Fifteen of these were followed up on, and all but 1 contained granular material under till cover. The preliminary ground follow-up results for 1 of the anomalies indicate a minimum of 1 million Mg of gravel that is covered and underlain by till. The test trials and routine surveying to date have shown that the E-Phase system can be used successfully for locating surficial and intertill granular deposits and that the system as it now exists represents a major advance in soil-exploration methods.

IN MANY areas, including Saskatchewan, all surface deposits of granular material have been exploited, and interest is turning to those covered with a considerable thickness of overburden. Conventional methods of interpretation by aerial photographs are not usually adequate for the location of these buried deposits. Ground geophysical measurements are useful but time consuming and costly unless they are applied to a specific and relatively small area. In 1967, the Department of Highways of Saskatchewan began an investigation of airborne geophysical survey methods for mapping shallow deposits of gravel. In 1968 and 1969, surveys were carried out by using the input airborne electromagnetic system. This system has a number of base-metal discoveries to its credit, but the trials with input indicated that an airborne system with better sensitivity was required to detect granular deposits. An airborne resistivity system called E-Phase was developed in 1970. The trials of the E-Phase system in 1970 and 1971 indicated that this system has the potential to detect buried deposits.

RESISTIVITY OF EARTH MATERIALS

The physical property of electrical resistivity of earth materials forms the basis of the resistivity method of geophysical subsurface investigation. Figure 1 shows a relationship between resistivity and unconsolidated sediments and rocks compiled from a number of sources (1, 2, 3). The resistivity of minerals, ores, rocks, and Pleis-

*Mr. Middleton was with Barringer Research Ltd. when this research was performed.

tocene materials varies between wide limits. Unconsolidated materials have resistivities that are lower than the resistivities of crystalline rocks but may overlap with resistivities of sedimentary rocks. There are 4 major factors that determine the resistivity of soils: type of soil, water content, soil temperature, and ice content. Type of soil is independent of time over long periods of time. However, water content, soil temperature, and ice content are subject to daily and seasonal variations. A number of less important factors, such as pressure and free-salt content of the pore water, also influence the resistivity of the soil strata (2). Gravel and sand tend to have high resistivity; organic material, silt, clay, and till have low resistivity because clay particles act as charge carriers.

E-PHASE METHOD THEORY

The E-Phase system is a passive system that uses radio wave transmissions to provide the exciting primary electromagnetic field; electrical properties of the ground are derived from measurements of the ground wave of the vertically polarized radio waves.

If the earth is assumed to be perfectly conducting, the measurement of the field components of a vertically polarized radio wave transmission would show that there is an electric field E that is vertical and a magnetic field H that is horizontal and perpendicular to the direction of propagation (Figure 2). If the resistivity of the ground increases from 0, then the electric field will be tilted forward in the direction of the propagation. The magnitude of the forward tilt is a function of the resistivity of the ground and the frequency of the transmission. Over resistive ground at low frequencies, such as 20 kHz, the wave tilt may be as much as 1 degree; however, over conductive ground, the wave tilt may be as little as a few minutes (decimal degrees) of arc. The electric vector, which is tilted because of the resistivity of the ground, has a vertical component E_z and a horizontal component E_x in the direction of propagation (Figure 3). To measure the tilt of the electric vector from an airborne platform is virtually impossible, but an indirect measurement of the tilt can be made by measuring the horizontal and vertical components of the electric field. Local changes in the resistivity of the ground cause variations in the amplitude and phase of the horizontal electric field. Measurements of these variations at or near the ground surface are the basis of the method. Variations in the vertical electric field and in the horizontal magnetic component occur near abrupt lateral changes in resistivity, but no significant variations take place when the resistivities change gradually. However, the horizontal electric field is dependent on the resistivity of a horizontally stratified ground and the measurement of this field is useful in mapping gradual variations in the resistivity and thickness of flat-lying strata (4). In the case of homogeneous half-space, if displacement currents (which are important only at high frequencies and resistivities) are ignored, the ratio of either the in-phase component $E_x(I)$ or the quadrature-phase component of the horizontal electric field $E_x(Q)$ and the vertical electric field E_z can be shown to be proportional to the square root of the resistivity (Figure 4). Because of theoretical and practical considerations, the E-Phase system measures the ratio of $E_x(Q)$ and E_z, and, therefore, the resistivity of the ground at 3 frequencies simultaneously. As a result of the assumption made (homogeneous half space, single uniform layer), the resistivity determined by the system in the case of layered earth is an apparent resistivity. The apparent resistivity is defined as the resistivity of that uniform half space (single homogeneous layer) that would give the same value for ratio $E_x(Q)/E_z$ as that which actually was measured (5, 6).

In the layered situation, which is the case under most geologic conditions, some information is lost by not measuring the in-phase component of the horizontal electric field, but this can be overcome to a large degree by measuring the quadrature-phase component at several well-separated frequencies. The depth penetration of the radio waves is dependent on the resistivity of the ground and the frequency of the transmission. The behavior of the skin depth (a measure of depth penetration) as a function of frequency is shown in Figure 5, which illustrates that the effective depth of investigation can be altered by changing the frequency. In Figure 5, ρ = resistivity in ohm-meters, f = frequency in hertz, and μ = permeability in henries per meter ($12.57 \times$

Figure 1. Resistivity of earth materials.

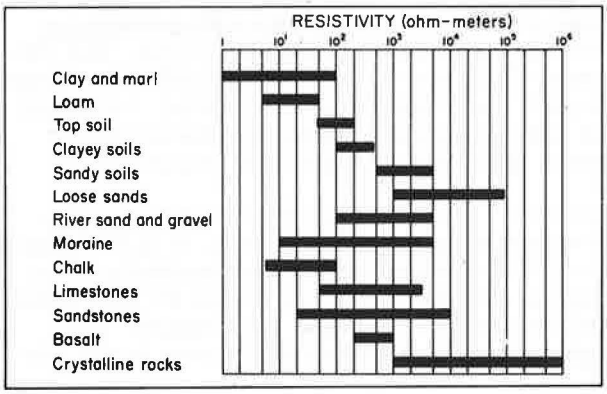

Figure 2. Field vectors for perfectly conducting earth, $\rho = 0$.

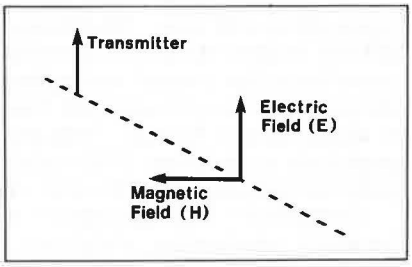

Figure 3. Field vectors for resistive earth $\rho = \rho_1$.

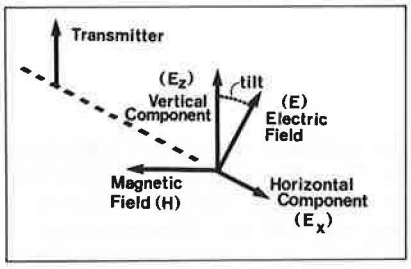

Figure 4. Relationship between electric field components and resistivity assuming uniform half space and ignoring displacement currents.

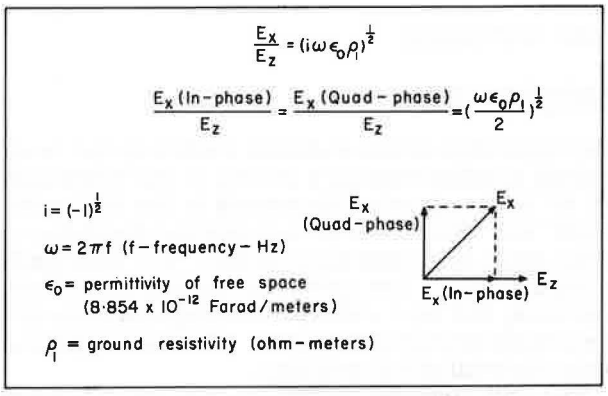

Figure 5. Skin depth as a function of resistivity assuming uniform half space and ignoring displacement currents.

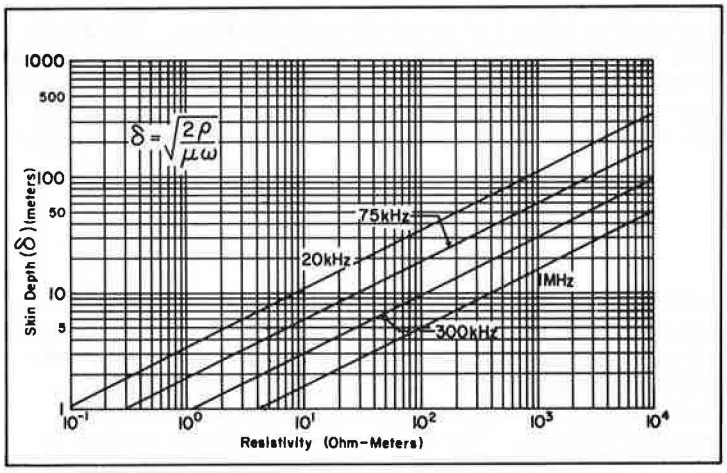

15^7 H/m). $\omega = 2\pi f$.

The deepest penetrating radio waves are in the very low frequency (VLF) range between 10 and 30 kHz. VLF transmissions provide communications with submarines, and the transmitters are operated by government agencies around the world. The frequencies in the second range, low frequency (LF), are between 200 and 400 kHz. These are aircraft navigational aid frequencies, and the transmitters are located at airfields or along airline routes. The shallowest penetrating radio waves are transmitted by amplitude modulation (AM) ratio stations in the broadcast band (BCB) range of frequencies between 550 kHz and 1100 kHz.

Because the VLF frequency is approximately 50 times that of the BCB frequency, the depth penetration, which varies as the square root of the frequency, is at VLF frequency approximately 7 times that at the BCB frequency for a given resistivity. One frequency of each of the 3 frequency bands is used for surveying and the electric fields are monitored simultaneously. In effect, results from 3 depths are obtained. By virtue of using 3 frequencies, the geologic section is described as 3 layers having distinct electrical properties.

Instrumentation can be installed in fixed-wing aircraft or in helicopters; the sensors will be located in a nose boom in both cases. The flight path of the aircraft is recorded by using a 35-mm camera. Fiducial marks are made automatically at 1-sec intervals on the flight path film, the analogue chart recorder, and the digital magnetic tape recording, which provides the means to relate the airborne records to the ground.

CASE HISTORIES

Kindersley Area

The application of the E-Phase method to locate granular material and map Pleistocene geology is illustrated by a survey in the Kindersley area (7). The survey was carried out in 1971, and only 1 frequency in the BCB range was used (540 kHz). The flying height was 75 m above ground, and the flight-line interval was 300 m. The direction of the flight lines was north-south. The main geological features of the area are shown in Figure 6 (8). The northeast-striking interlobate moraine, the ground moraine in the southeast, and the northwest-striking meltwater channel are the promising areas for occurrence of gravel deposits. The rest of the survey area is covered by glacial lake basin material of till and clay.

The BCB-apparent resistivity contour map shown in Figure 7 illustrates the striking correlation between the known geology and the apparent resistivity contours. The interlobate moraine, ground moraine, and meltwater channel are outlined by resistivities ranging up to 1000 $\Omega \cdot m$. The glacial lake basin material correlates with the low apparent resistivities. Note the higher resistivity area in the northwest corner of the area that may indicate a buried moraine hitherto unknown. Two areas were selected for a ground follow-up that consisted of holes 8 m apart along flight lines. The depth of the holes was 8 m. A definite correlation was found between the resistivity and soil texture: The higher the resistivity was, the coarser the soil was. Although an apparent resistivity that is characteristic of the type of soil in an area may not be appropriate for another area, definite limits of resistivity can be assigned for broad ranges of soil classification (7).

Wadena Area

The 1971 trials with E-Phase led to a full-scale gravel-search program in 1973. The search concentrated on intertill deposits (layers of sand or gravel sandwiched between 2 till sheets). A wide area is known to contain these deposits running in a northwest-southeast direction through southern Saskatchewan. Because of the thickness of the overburden or upper till sheet, the deposits are effectively masked to conventional aerial-photograph or ground-search methods. The ability of the E-Phase method to

Figure 6. Surficial geology of Kindersley area.

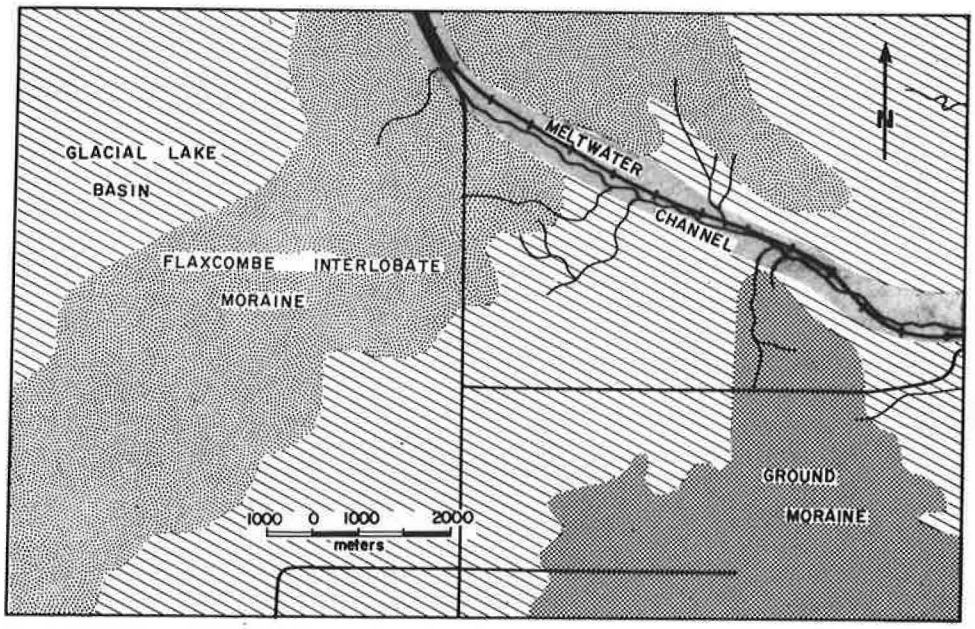

Figure 7. Broadcast-band-apparent resistivity contour map for Kindersley area.

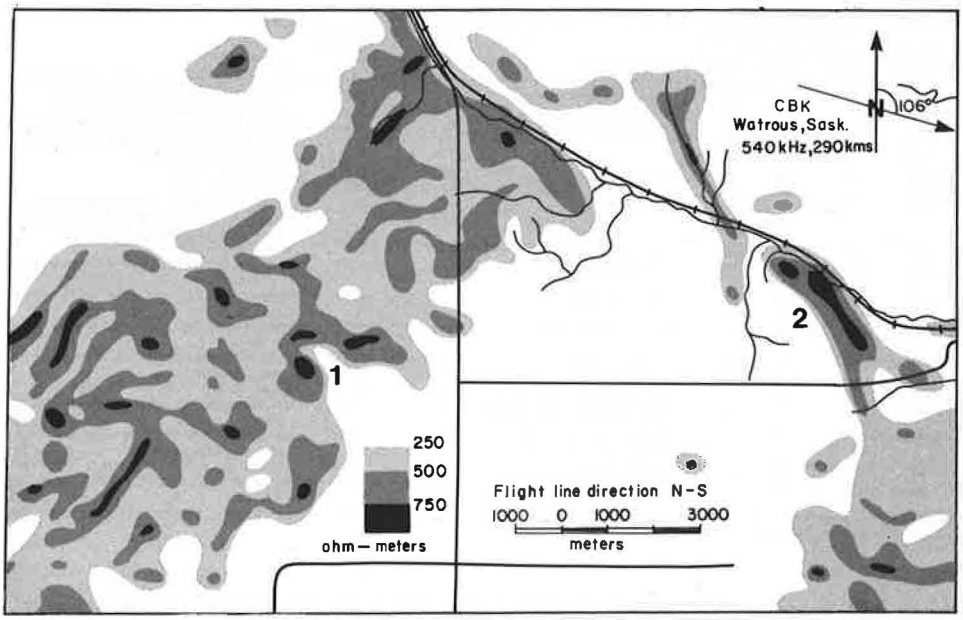

cover a wide area in a short time and sense through a significant depth makes these deposits available for exploration.

The area surveyed in this case is near Wadena and covers about 464 km^2. The flight-line spacing was 400 m; the aircraft kept a constant altitude of 75 m; and 966 line km were required to cover the area. The 3-frequency system was used, and apparent resistivities at 3 frequencies were obtained simultaneously. An initial check

Figure 8. Low-frequency-apparent resistivity contour map for Wadena area.

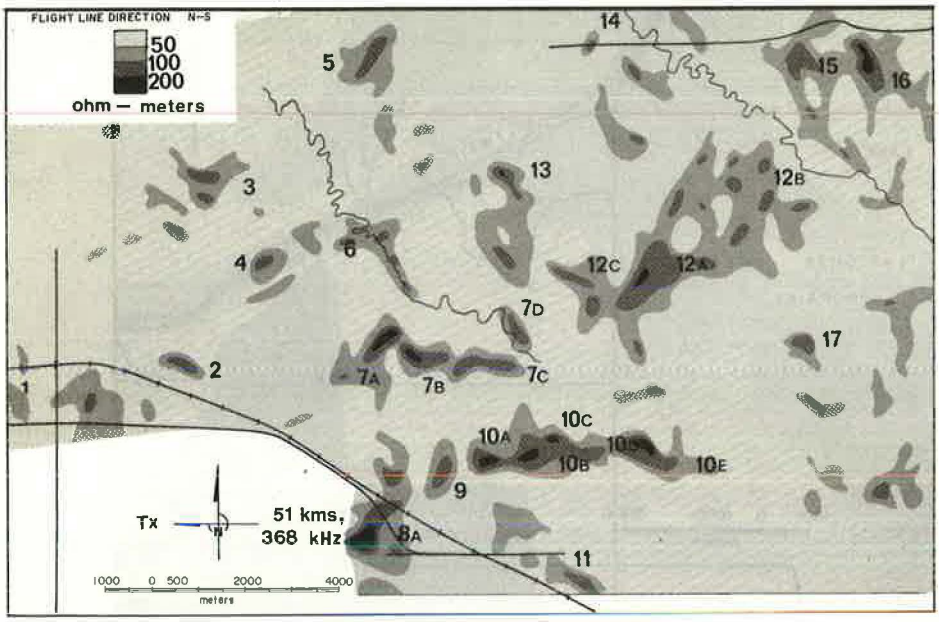

Table 1. Summary of ground follow-up for Wadena area.

Anomaly	Drill Holes	Total Meters	Percentage of Materials			Photogeology	Flight Lines Crossed	Max. LF Anomaly (Ω·m)	Remarks
			Gravel	Sand	Other				
2	10	73	30	44	26	Likely old beach ridge	1	<150	Anomalous on 3 frequencies; 1 hole bottoms in gravel.
5	32	237	43	4	53	Small area of surficial sand	2	125	Gravel and coarse gravel: approximately 10^{5} Mg; water table: ~4m; number of holes bottom in gravel.
7A	18	110	3	43	54	Surficial granulars	3	>150	Water table: ~2m.
7C	18	110	3	43	54	Surficial granulars	3	>150	Water table: ~2m.
8A	9	55	—	7	93	No indications	1	350	Resistivity may have been affected by topography. Could not be tested along flight line because of topography.
9	12	67	33	6	61	Terrace and outwash	1	200	Water table: >5m.
10C	32	192	—	64	36	Surficial granulars	2	200	Water table: 7m; number of holes bottom in sand.
10D	32	192	—	64	36	Surficial granulars	1	200	Water table: 7m; number of holes bottom in sand.
10E	32	192	—	64	36	Surficial granulars	3	275	Water table: 7m; number of holes bottom in sand.
11	6	34	—	21	79	No indications	1	225	Peak of anomaly could not be checked because of access.
12A	36	272	51	19	30	No indications	4	200	Mostly fine gravel; water table: ~6m.
12B	26	186	26	54	20	Small area of surficial sand	1	175	1 hole bottoms in sand; 1 hole bottoms in gravel.
13	6	37	—	2	98	Surficial sand in vicinity	1	175	Anomaly is not fully explained; source may possibly be deeper.
14	7	46	21	39	40	Old beach ridge	1	125	Fine gravel and sand; water table: ~2m.
15	8	41	—	15	85	No indications	1	150	Poorly defined anomaly; water table ~4.5m.

Note: Other materials include till, silt, sandy silt, and topsoil.

of the computed apparent resistivities indicated that the most diagnostic information is contained in the LF-apparent resistivity data. A contour map was prepared for this frequency (Figure 8), but all 3 apparent resistivities were used for interpreting the data (9). (Anomaly 5 in Figure 8 is recommended for follow-up.)

The background resistivity is about 50 Ω·m or less, which indicates the upper till cover. In anomalous zones, the apparent resistivities may exceed 300 Ω·m. Twenty-seven specific resistivity anomalies were recommended for ground checking, but only 15 anomalies were actually checked. Two hundred and two holes were dug to an average

depth of 10 m (10). A summary of the results of the ground follow-up is given in Table 1. In all cases except one (anomaly 13), gravel or sand or both were found overlain by till or silt and underlain by till. A number of the anomalies can be correlated with photogeological indications (anomalies 5 and 12B). In most of the cases the LF-apparent resistivity was the most anomalous; the BCB-apparent resistivity was somewhat lower. The VLF-apparent resistivities are the least anomalous of the 3 apparent resistivities. The depth to the water table varied considerably throughout the area and no definite conclusions can be made of its effect on apparent resistivity. For anomaly 13, only a minor amount of sand was found, which does not sufficiently explain the anomaly. Increased resistivity of the covering material or a more resistive material at depth or both may explain the anomaly. Anomaly 8A, in which only minor sands were found, could not be checked at the peak of the anomaly because of access problems. Steep topography may also have affected the apparent resistivities at this location.

Anomaly 5 is of particular interest (Figure 9). Photogeological study indicated a small area of surficial sand southeast of the main peak of the anomaly. Thirty-two test holes were drilled and the results are given in Table 2. The resistivity contours suggest that the intertill deposit may extend to the south of holes 4 and 5 and to the northeast of holes 1, 3, and 4. The bulk of the deposit is located between flight lines; however, sufficient granular material is located along flight line 31 to give an indication of a possible deposit (Figure 10). The LF-apparent resistivity is much higher along the flight line, which indicates a change in the composition of surface and near surface materials. The LF-apparent resistivity contours by no means map out exactly the area of the intertill deposit, but they at least give an indication of where it is located. This deposit would not have been located by the usual location methods used previously in Saskatchewan. Preliminary checking indicates that a minimum of 1 million Mg of gravel may exist in this deposit. This will probably pay for the cost of surveying (10).

Anomaly 12A is also of interest (Figure 11). Aerial-photograph interpretation indicated no surficial sand or gravel. Thirty-six holes were drilled over the anomaly, and granular material was located in each hole. The granular material (fine gravel and sand) is covered by an average of 1.25 m of top soil and till, and the deposit is underlain by till. The profiles of apparent resistivity and drilling results shown in Figure 12 for flight line 47 clearly indicate the usefulness and necessity of using 3 frequencies. The BCB resistivity is lower than the LF-apparent resistivity because of the much lower true resistivity of the upper till. The BCB waves apparently just penetrated into the gravel. VLF waves penetrate much deeper and show the effect of the high-conductivity substratum till; the combined effect of the low resistivity of the upper and bottom till counteracts the higher resistivity of the intertill gravel, which results in the low VLF-apparent resistivities. LF radio waves penetrate into the gravel, and the high apparent resistivities obtained at the LF frequency diagnostically describe the intertill deposit in this geologic environment. The gravel deposit could have been missed by using the VLF frequency only.

Computer programs and 3-layer interpretation curves were developed to model the 3-layer resistivity distribution (11). The method was applied to the data along flight line 47 at 2 locations. The apparent resistivities computed from the assumed true resistivities and thicknesses agree with the observed apparent resistivities at both locations. The northerly location is close to hole 2, and the thicknesses of the layers used in the computation of apparent resistivities are in good agreement with the observed thicknesses in hole 2. The computer model located south of hole 32 indicates an extension of the granular deposit that has not yet been drilled. A true resistivity of 40 $\Omega \cdot m$ for the upper till and 10 $\Omega \cdot m$ for the bottom till is within the range of resistivities of tills. The 1000 $\Omega \cdot m$ true resistivity of the intertill deposit complex provides a good resistivity contrast between it and the surrounding, covering, and underlying till (Figure 12).

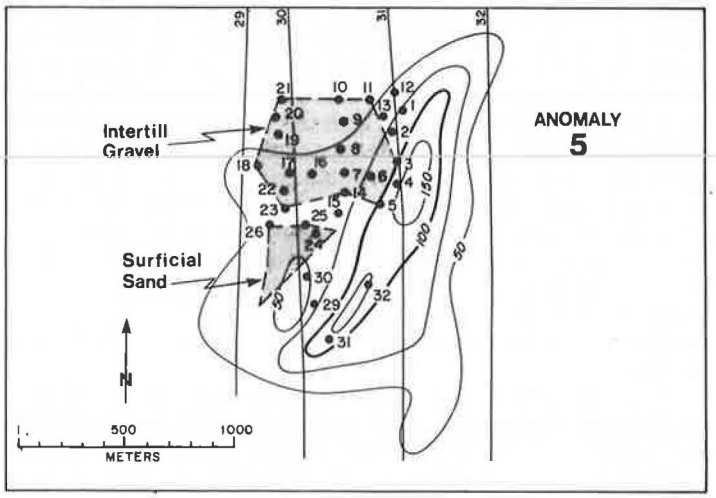

Figure 9. Low-frequency-apparent resistivity contours and drill-hole locations for anomaly 5 in Wadena area.

Table 2. Drilling results for anomaly 5 in Wadena area.

Hole Number	Stratigraphy Thickness (m)	Type	Thickness (m)	Type	Thickness (m)	Type	Thickness (m)	Type	Water Table (m)	Remarks
1	0.3	Sand	4.9	Till	3.3	Gravel	0.3	Till	5.5	
2	4.3	Till							–	Rock? at 4.6 m
3	3.0	Till	4.0	Gravel	0.3	Till			3.6	
4	2.9	Till	6.9	Gravel	0.6	Till			3.6	
5	4.6	Till	4.3	Sand					4.9	Bottom sand
6	0.6	Sand	1.8	Till	5.8	Gravel	0.6	Till	3.0	
7	0.6	Silty sand	1.5	Till	6.7	Gravel			3.0	Bottom gravel
8	2.1	Till	6.1	Gravel	0.3	Till			2.4	
9	2.4	Till	6.7	Coarse gravel					3.0	Bottom gravel
10	2.4	Till	6.1	Coarse gravel					3.0	Bottom gravel
11	3.6	Till	1.8	Gravel	2.1	Till			3.7	
12	5.8	Till							–	
13	5.8	Till							–	
14	2.1	Till	6.7	Fine gravel					3.0	Bottom gravel
15	5.2	Till							–	
16	2.1	Till	4.6	Fine gravel	0.6	Till			3.0	
17	1.0	Till	4.6	Gravel	0.3	Till			3.0	
18	1.5	Till	0.6	Gravel	3.6	Till			2.1	
19	1.2	Till	0.9	Sand	4.6	Gravel	0.6	Till	3.0	
20	1.2	Till	6.1	Fine gravel					3.0	Bottom gravel
21	3.0	Till	4.3	Fine gravel					3.0	Bottom gravel
22	1.2	Till	5.8	Fine gravel					3.0	Bottom gravel
23	3.0	Till	4.3	Sand					3.0	Bottom gravel
24	1.8	Sand	5.5	Till					–	
25	0.9	Gravel	4.9	Till					–	
26	0.6	Gravel	5.2	Till					–	
27	0.9	Gravel	4.9	Till					–	
28	2.4	Till	4.6	Gravel	0.3	Till			5.2	
29	2.7	Till	4.6	Gravel						Bottom gravel
30	3.7	Till	1.5	Sand	5.2	Fine gravel			4.9	Bottom gravel
31	5.2	Till								
32	5.8	Till								

Note: Thickness of topsoil is 0.3 m in each hole.

CONCLUSIONS

The earlier surveys indicated that the E-Phase system could be used for location of surficial granular deposits. Recent surveys show that the system can be used with confidence to locate buried intertill deposits. This is a significant step forward in locating these important deposits.

The E-Phase airborne resistivity system appears to be a unique method that has many potential applications such as locating permafrost, outlining areas of shallow bedrock, exploring groundwater, and locating granular material. The test trials and routine surveying to date have shown that the E-Phase airborne resistivity system can be used successfully for locating surficial and intertill granular deposits. More

Figure 10. Very-low-frequency-, low-frequency-, and broadcast-band-apparent resistivity profiles and drilling results for anomaly 5 in Wadena area.

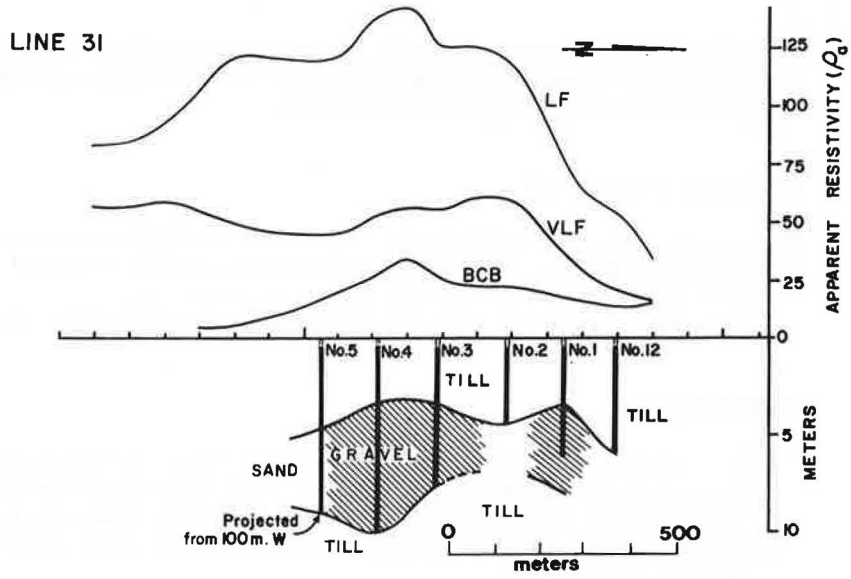

Figure 11. Low-frequency-apparent resistivity contours and drill-hole locations for anomaly 12A in Wadena area.

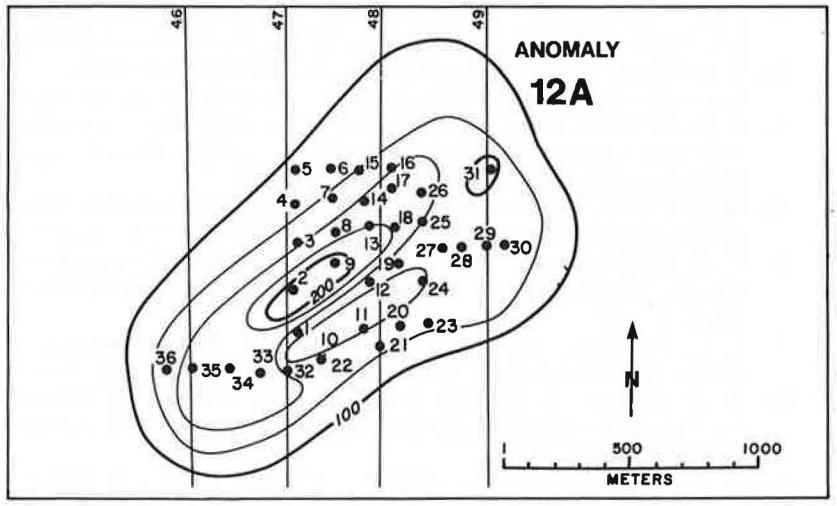

Figure 12. Very-low-frequency-, low-frequency-, and broadcast-band-apparent resistivity profiles, and drilling and computer modeling results for anomaly 12A in Wadena area.

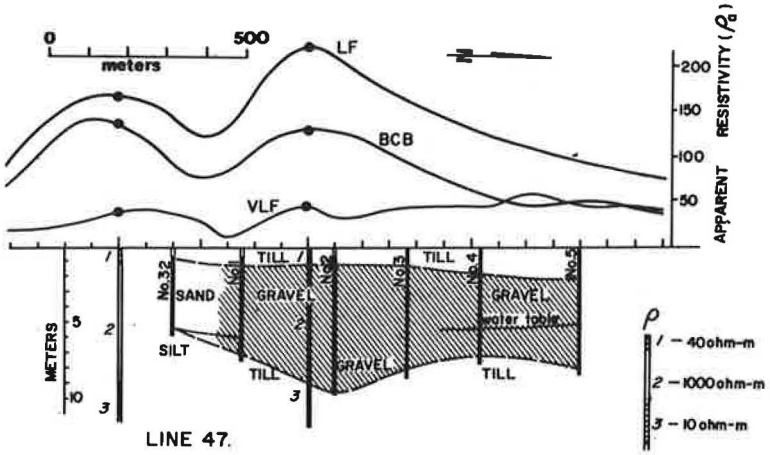

experience and data are required to refine operational specifications for given areas and to refine interpretation techniques, but the system as it now exists represents a major advance in soil exploration methods.

ACKNOWLEDGMENTS

We wish to thank the Saskatchewan Department of Highways and Transportation for permitting the data to be published and for the department's offer to make Technical Report 21 available to anyone who wishes to receive it.

E-Phase and Input are registered trademarks of Barringer Research Ltd.

REFERENCES

1. P. Hoekstra, P. V. Sellmann, and A. J. Delaney. Airborne Resistivity Mapping of Permafrost Near Fairbanks, Alaska. Cold Regions Research and Engineering Laboratory, U.S. Army Corps of Engineers, Hanover, N. H., Research Rept. 324, 1974.
2. C. A. Heiland. Geophysical Exploration. Hafner Publishing Co., New York and London, 1963.
3. D. S. Parasnis. Physical Property Guide for Rocks and Minerals. Atlas Copco ABEM, Stockholm, geophysical memorandum, April 1971.
4. F. C. Frischknect. Electromagnetic Scale Model Studies of Geophysical Methods Using Plane Wave Source. Univ. of Colorado, PhD dissertation, 1973.
5. J. R. Wait. Electromagnetic Waves in Stratified Media. Macmillan Co., New York, International Series of Monographs on Electromagnetic Waves, Vol. 3, 1962.
6. J. D. McNeill, F. L. Jagodits, and R. S. Middleton. Theory and Application of the E-Phase Airborne Resistivity Method. Symposium on Exploration Electromagnetic Methods, Univ. of Toronto, Abstract, 1973.
7. R. W. Culley. Use of Airborne Resistivity Surveys for Gravel Location. Canadian Mining and Metallurgical Bulletin, Vol. 66, No. 731, May 1973.
8. E. A. Christiansen. Geology and Groundwater Resources of the Kindersley Area (72-N), Saskatchewan. Geology Division, Saskatchewan Research Council, Regina, Rept. 7, 1965.
9. F. L. Jagodits. Report on the Airborne E-Phase Surveys, Cowan Lake and Wadena Areas, Saskatchewan. Barringer Research Ltd., Aug. 1973.
10. R. W. Culley. Evaluation of an Airborne Resistivity Measurement System (E-Phase) for Gravel Location. Saskatchewan Department of Highways and Transportation, Technical Rept. 21.
11. G. J. Palacky and F. L. Jagodits. Computer Data Processing and Quantitative Interpretation of Airborne Resistivity Surveys. Geophysics, 1974.

REMOTE SEISMIC DETECTION BY LASER INTERFEROMETER FOR MINING GEOPHYSICS AND TUNNELING OPERATIONS

G. L. Fitzpatrick and R. A. Bruce, Denver Mining Research Center,
U.S. Bureau of Mines

A modified laser interferometer system is developed that makes possible the noncontact detection and analysis of dynamic displacements on remote, unprepared rock surfaces. The system is a broadband device and does not suffer from acoustic-impedance-matching problems or frequency-response problems characteristic of conventional contact transducers. The potential applications of such a system include hazard detection in mines, seeing ahead of a working face in tunneling operations, vibration-mode studies of large structures, and examination of vibrating surfaces in hostile environments.

•MANY problems in mining geophysics may be solved by employing seismic techniques. By using geophones or other contact transducers as receivers and various seismic sources, one may perform vibration analyses on rock structures, measure P- or S-wave velocity profiles, and perform experiments such as seismic holography (1, 2) to detect cavities, inclusions, or fracture zones in rock ahead of working faces or in pillars.

Contact measurements of the type described have several drawbacks. First, and most obvious, such measurements always involve the fixing or cementing of a transducer or transducers to the surface of interest. Cables, preamplifiers, and other paraphernalia are often required to transmit and record received signals. These measurements are time consuming, expensive, and obtrusive because they frequently interfere with work in progress. In almost all cases in which a remote observer has line-of-sight access to the surface of interest, one may employ a new technique based on laser interferometry that has none of the forgoing disadvantages and a considerable number of advantages.

Conventional laser interferometric techniques have been applied to the problem of remotely detecting motions of rock or other structural surfaces. However, these conventional techniques invariably use a remote retroreflector fixed to the surface under study. A laser beam from the observer's position is directed toward the retroreflector, and the returned beam is compared interferometrically with the outgoing beam. Phase variations in the returned beam that are due to Doppler shifts resulting from changes in the position of the surface are converted by the interferometer into a series of moving interference fringes that completely characterize line-of-sight motions of the surface. Using an interferometer in this way is clearly disadvantageous because it is not a truly remote measuring system because a retroreflector must be placed and cemented at the point of interest. The potential of interferometry for truly remote noncontact measurements (no retroreflector, geophone, on the like) is thereby lost.

The purpose of this paper is to report on a new interferometric method for remotely detecting vibrations on unprepared rock surfaces and to outline briefly how such a system might be used in various mining or tunneling situations. Our principal goal will be not to provide a detailed account of these applications but rather to demonstrate that such a system is feasible. After demonstrating the feasibility of the system, we will discuss applications, including many that are relevant to tunneling and underground excavation in general.

The method described in this paper is truly remote because the observer located

at the laser interferometer may direct a laser beam to some unprepared remote surface and make measurements of its dynamic behavior. In brief, the action of the remote retroflector in amplifying the returned signal is performed by a 6-in. (15.24-cm) light-gathering telescope located at the position of the interferometer. This telescope amplifies the low-intensity scattered light from the remote surface and focuses the outgoing laser beam in a diffraction-limited spot on the surface to be sampled. The returned light signal is mixed with the outgoing signal as is done in the conventional interferometric devices, and fringes characterizing the motion are detected.

BACKGROUND

In the course of applying acoustic holography to the problem of imaging voids and other discontinuities in rock by using seismic waves (1, 2), we encountered the practical difficulty of recording seismic data when using 2-dimensional detector arrays that involve large numbers of elements. To reduce the time involved in recording such data, we considered various noncontact measurements. In particular, we considered the technique of pulsed laser holographic interferometry, which is a remote technique that involves no prior preparation of the surface. However, to determine the time history of a given surface, we would need a time sequence of holographic interferograms. Apart from the practical difficulties of this requirement, the difficulty of data interpretation that is caused by nonlocalized fringes is also present. However, the fact that holographic interferometry would work in principle meant that any kind of interferometry would work. These considerations led ultimately to the work reported here.

THEORY OF OPERATION

In this section, we present a simple theoretical analysis of the problem of optically detecting and analyzing displacements of moving surfaces. We first examine surfaces moving with a constant velocity along the line of sight; then we take up the general case of sinusoidal and arbitrary motion. Doppler shifts and various effective coherence considerations also are discussed.

Interferometers With Moving "Mirrors"

If a laser beam is directed toward some moving surface of interest, a "mirror" (it can be completely rough), the reflected component returned to the position of the laser will have a circular frequency given by the relativistic Doppler formula

$$\omega = \frac{\omega_o(1 \pm 2v/c)}{\sqrt{1 - v^2/c^2}} \tag{1}$$

where

- v = velocity along the line of sight (+v refers to a mirror approaching a stationary interferometer,
- ω_o = stationary laser frequency, and
- c = light velocity in vacuum (~ air velocity neglecting turbulent effects).

Because $v \ll c$ for most applications, this expression may be approximated by the usual classical result

$$\omega = \omega_o(1 \pm 2v/c) \tag{2}$$

or simply

$$\left|\frac{\Delta\omega}{\omega_o}\right| \sim 2v/c \tag{3}$$

Thus light of 2 different frequencies will mix in the interferometer, and the problem is to determine the observed interference field. If we assume for now that the reference frequency ω_o is time stable and that the reference beam is perfectly monochromatic, then the instantaneous amplitude at the interferometer for a source moving at constant velocity will be

$$A(t) = A_s \exp(-i\omega t) + A_o \exp(-i\omega_o t) \tag{4}$$

Because only square law detectors of light signals are possible, we have the corresponding instantaneous intensity

$$I(t) = A^*(t)A(t) = A_s^2 + A_o^2 + 2A_sA_o\cos[(2v/c)\omega_o]t \tag{5}$$

where, without loss of generality, we have assumed the source amplitude A_s and the reference amplitude A_o to be real numbers, and where v is the line-of-sight velocity as before.

For a given value of v, the observed beat frequency between the 2 light beams $|\Delta\omega| \sim (2v/c)\omega_o$ clearly places limits on the response time of any detector that might be used to record I(t). For constant v, the instantaneous intensity (assuming a perfect detector) would look as shown in Figure 1. In Figure 1, the quantity $(v/c)\omega_o$ is the Doppler or fringe frequency where ω_o is the optical laser frequency and c is the speed of light. The period of I(t) is $\tau \sim (2\pi/|\Delta\omega|) \sim (\pi c/v\omega_o)$, and if the response time of the detector, call it T, is 0.1τ or less, such a detector clearly would be capable of recording I(t) directly. We shall discuss this point in more detail later. For the present, that $T \leq 0.1\tau$ and that I(t) is measured directly will be assumed. The important feature about Figure 1 is that the beat frequency or Doppler frequency shift $|\Delta\omega|$ is directly proportional to the magnitude of the line-of-sight velocity v.

Sinusoidally Moving " Mirrors"

Consider a surface moving with a sinusoidal line-of-sight particle velocity given by

$$v = v_o' \sin(\omega_o' t) \tag{6}$$

where

v_o' = peak particle velocity of the surface, and
ω_o' = circular frequency of the surface vibration.

The corresponding Doppler shift of the light beam that samples this motion is (equations 3 and 6)

$$\Delta\omega \sim 2(\omega_o/c)\, v_o' \sin(\omega_o' t) \tag{7}$$

In this case, $\Delta\omega$ is not a constant, and the formula of equation 5 for intensity is no longer valid. Writing the total complex amplitude in the interferometer as

$$A = A_o \exp[-i\theta_o(t)] + A_s \exp[-i\theta_s(t)] \tag{8}$$

where $\theta_o(t)$ and $\theta_s(t)$ = phase angles to be determined, we note as before that $\theta_o(t) = \omega_o t$. However, the phase angle $\theta_s(t)$ is now a more complicated time-varying phase because $\Delta\omega$ is a function of time. Therefore, because

$$\frac{d\theta_s(t)}{dt} = \omega_s(t) \tag{9}$$

and

$$\omega_s = \omega_o + \Delta\omega \tag{10}$$

$\theta_s(t)$ is given by

$$\theta_s(t) = \int \omega_s dt = \int \omega_o dt + \int \frac{2\omega_o}{c}\, v_o' \sin(\omega_o' t)\, dt \tag{11}$$

$$\theta_s(t) = \omega_o t - 2\,\frac{\omega_o v_o'}{c\omega_o'} \cos(\omega_o' t) \tag{12}$$

or

$$\Delta\theta = \theta_s(t) - \theta_o(t) = -2\,\frac{\omega_o v_o'}{c\omega_o'} \cos(\omega_o' t) \tag{13}$$

By using equations 8 and 13, one finds the time-varying fringe signal for a sinusoidally moving surface to be

$$I(t) = A_s^2 + A_o^2 + 2A_s A_o \cos\left|\frac{2\omega_o v_o'}{c\omega_o'} (\cos\omega_o' t)\right| \tag{14}$$

Figure 2a shows this intensity $v_s t$; Figures 2b, 2c, and 2d show corresponding Doppler shift, surface velocity, and surface displacement respectively. Two principal features of I(t) should be noted. First, I(t) is a periodic function having a period $2\pi/\omega_o'$ where ω_o' = circular frequency of the oscillating surface. Second, the maximum beat frequency contained in I(t), namely $v_o' \omega_o/c$, will occur when v reaches its maximum value or when $\sin\omega_o' t = 1$. At this time,

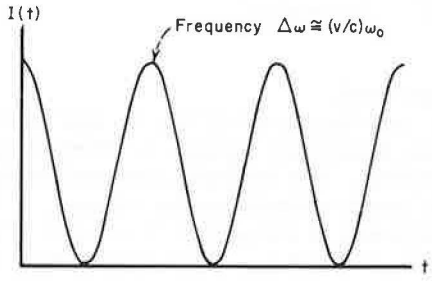

Figure 1. Time-varying interferometer signal for a surface moving with a constant velocity along the line of sight toward or away from the interferometer.

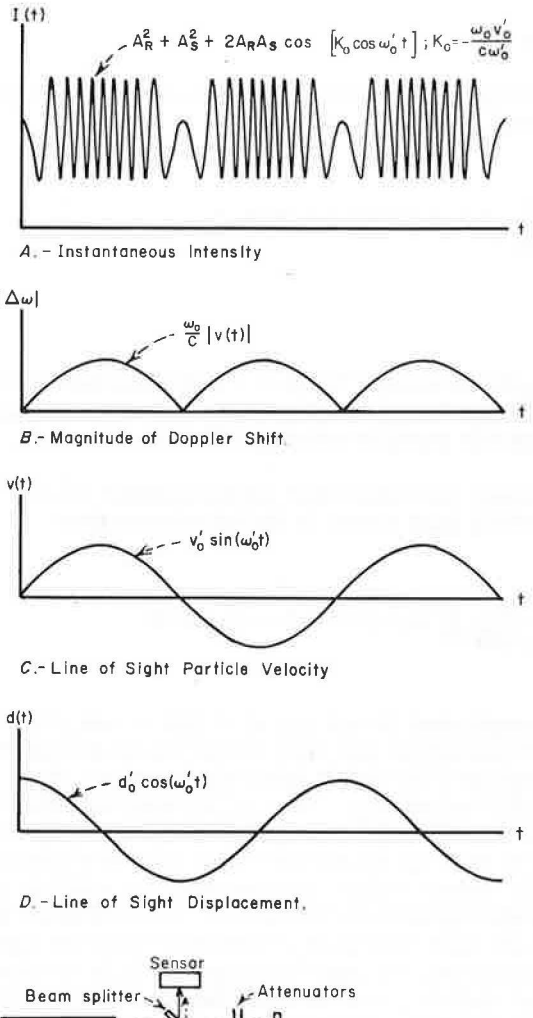

Figure 2. Characteristics of sinusoidally oscillating surface.

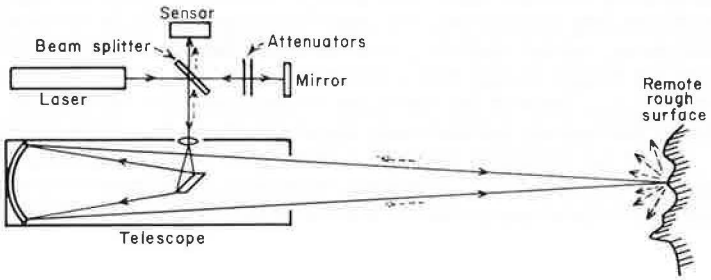

Figure 3. Schematic design of experimental apparatus.

$$|\Delta\omega| = (\omega_o/c)v_o' = (\omega_o/c)d_o'\omega_o' \tag{15}$$

where d_o' = peak displacement.

By measuring $|\Delta\omega|$ and the period of I(t), we can determine all relevant parameters of the sinusoidal motion, namely v_o', d_o', and ω_o'. There are alternate ways to analyze I(t) to get the same information. For example, because the interference fringes occur at intervals of $\lambda_o/2$ of the surface displacement where λ_o = optical wavelength, a simple count of the fringes contained in one period of I(t) will be enough to determine the peak surface displacement d_o'. If there are N fringes in one period of I, there are N - 1 fringe spaces corresponding to a total distance $2d_o' = [(N - 1)/2]\,\lambda_o$.

General Motion

In the most general case, the line-of-sight surface motion may be characterized as a Fourier synthesis

$$v(t) = \frac{1}{\sqrt{2\pi}} \int A_v(\omega_o') \exp(-i\omega_o' t)\, d\omega_o' \tag{16}$$

where

ω_o' = a given circular frequency of the surface motion, and
$A_v(\omega_o')$ = an amplitude (velocity amplitude) at the frequency ω_o' chosen in such a way that the particle velocity v(t) is always real.

Following the same procedure that led to equation 13, one finds the phase difference $\Delta\theta(t)$ between the 2 light waves in the interferometer

$$\Delta\theta(t) = \frac{\omega_o}{c\sqrt{2\pi}} \iint A_v(\omega_o') \exp(-i\omega_o' t)\, d\omega_o'\, dt \tag{17}$$

where the corresponding fringe signal is just $\sim \cos[\Delta\theta(t)]$.

Note that, if $\cos[\Delta\theta(t)]$ has been recorded, $\Delta\theta(t)$ can be extracted up to a constant phase factor such as $2N\pi$ with N integral; therefore, $d/dt\,[\Delta\theta(t)]$ can be calculated. Because $d/dt\,[\Delta\theta(t)]$ is just $\Delta\omega = [2v(t)\omega_o]/c$, one can extract the particle motion [velocity v(t)] by calculation of the fringe signal $\cos[\Delta\theta(t)]$. If desired, one can Fourier analyze this, integrate to find the displacement, or take derivatives to find the acceleration. The point we wish to stress is that, in principle, any arbitrary interferometer fringe signal I(t) can be completely analyzed to determine all relevant factors corresponding to an arbitrary line-of-sight motion of an optically sampled surface. As far as line-of-sight motions are concerned, the interferometer is fully as useful as a contact transducer. However, unlike ordinary contact transducers that have finite bandwidth response, the optical fringe signal has unlimited bandwidth in that $\Delta\omega$ can be 0 to $\sim 10^{14}$ Hz. A very large $|\Delta\omega|$ cannot be recorded or examined by electronic devices; therefore, a practical, but hardly deleterious, upper limit on $\Delta\omega$ does exist.

That the forgoing method of detecting surface motions is noninterfering should be clear. No acoustic-impedance-matching problems commonly encountered in the use of contact transducers and no mechanical-response problems exist.

INITIAL DESIGN CONSIDERATIONS

To realize a practical system based on the forgoing theoretical ideas, a sufficiently intense return beam must be possible. Surface parameters such as reflectivity and roughness may not be altered for a remote system measurement; therefore, we have at our disposal 3 variables: detector sensitivity, light-gathering aperture, and laser intensity.

By increasing the size of the light-gathering aperture, increasing the laser power, and using a detector of sufficient sensitivity, one can enhance the signal-to-noise ratio of the returned signal. Other more subtle things can be done to improve the system. However, by optimizing these parameters for any system, one will optimize the quality and usefulness of the returned signal.

EXPERIMENTAL RESULTS

In this section, laboratory experiments are described that illustrate both the feasibility of making interferometric measurements of dynamic displacements on remote unprepared surfaces and the feasibility of performing various field tests.

Experimental Apparatus

Figures 3 and 4 show the schematic design and the actual system of the experimental apparatus. Further details of the experimental design may be found elsewhere (3). Basically, the system consists of a simple Newtonian reflecting telescope with a 6-in.-diameter (15.24-cm-diameter) f/4 parabolic mirror, 4-mw helium-neon (He-Ne) laser, and Michelson interferometer. The telescope both sends and receives the laser light, and the Michelson interferometer analyzes the scattered light. Various sensors including photomultipliers were used, but, for the experiments reported here, a simple solid-state detector was employed.

An examination of equation 5 or equation 14 shows that a large value of A_o will make the amplitude of the cross term that includes the desired signal large. The ability of the solid-state devices to safely operate in the presence of intense reference beams is one important advantage of the solid-state detectors over photomultipliers. For many of the applications envisioned for the interferometer, the ambient light levels may be too high to safely employ photomultiplier detectors.

Tests

Figure 5 shows interferometer output (upper trace) for a scotchlite target oscillating at 1 kHz (lower trace) 6 m from the interferometer. The qualitative similarity of the upper trace with the corresponding theoretical predictions shown in Figures 2a and 2d is evident. There are roughly 11 fringes for each period of the upper trace in Figure 5; therefore, the peak-to-peak displacement is about 5λ or about 3 μm. Evidently shorter optical wavelengths would improve this measurement.

The test shown in Figure 6 was performed to determine whether a signal could be obtained from a rough, unprepared surface moving in some complex way. The upper trace of Figure 6 represents the interferometer ouput from the rough unprepared surface of a struck limestone block 1 m in length located 6 m from the interferometer. The lower trace represents the simultaneous piezoelectric detector output at about 3 kHz resulting from a hammer blow signal propagating through the block. The piezoelectric crystal was located at a point several centimeters from the focus of the laser beam.

Because piezoelectric transducers tend to respond primarily to accelerations and because they have poor frequency response compared to the interferometer, a detailed comparison of the traces is not feasible. In making such tests, the block occasionally

suffered a small translation that was not recovered. The interferometer output is sensitive to this translation, but the peizoelectric transducer is unaffected by uniform translation. Nevertheless, from the basic success of such tests, noncontact velocity measurements that use the interferometer to detect first motion are certainly feasible, and, if no net translation is suffered by a surface, a complete analysis of the line-of-sight motion is possible.

The last test, which is shown in Figure 7, was performed by using very poor optical surfaces as targets to demonstrate the ability of the system to operate over large distances. The upper trace illustrates the interferometer output from an anthracite coal sample being driven sinusoidally at 30 Hz with a peak-to-peak line-of-sight displacement of about 15λ (9 μm) and located 100 m from the interferometer. The lower trace represents system noise with the laser beam blocked. The apparent amplitude modulation of the interferometer signal is due to variations in surface reflectivity as the coal sample moves.

It is clear from the foregoing results that truly remote measurements of surface vibration are feasible. However, certain limitations of the technique must be considered.

LIMITATIONS OF METHOD

In the forgoing sections, we deferred consideration of certain constraints and limitations imposed on the technique of interferometrically measuring surface displacements. In this section, we address these important points.

Effective Coherence

The generalized partial coherence factor (4) for 2 complex wave amplitudes A_1 and A_2 may be written as

$$\gamma = \frac{\langle A_1 A_2^* \rangle}{\langle A_1 A_1^* \rangle^{1/2} \langle A_2 A_2^* \rangle^{1/2}} \tag{18}$$

where

averaging operation $\langle\ \rangle$ = time average $\langle x \rangle = \frac{1}{2T} \int_{-T}^{+T} x \, dt$, and

T = an arbitrary time.

By writing the complex amplitudes at some fixed point as

$$A_1 = A_1^\circ \exp(-i\omega_1 t) \tag{19}$$

and

$$A_2 = A_2^\circ \exp(-i\omega_2 t) \tag{20}$$

where A_1° and A_2° are real numbers, one can show that, when ω_1 and ω_2 are constants, equation 18 reduces to

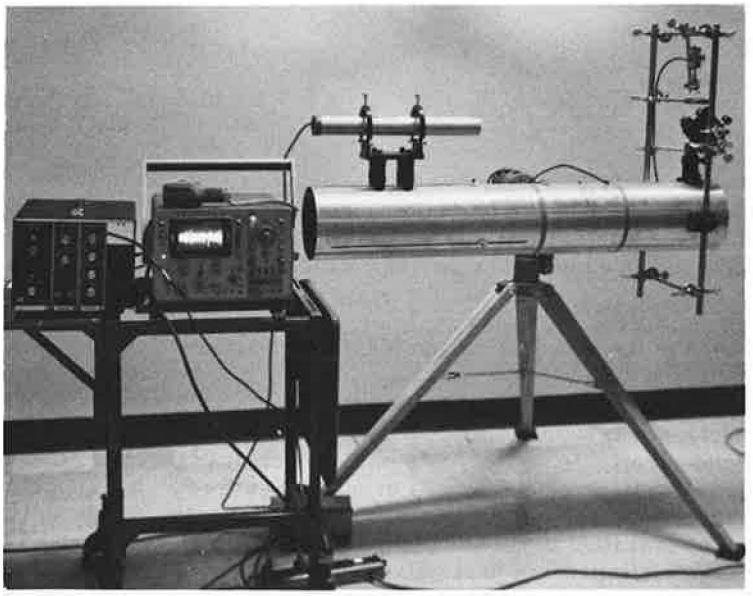

Figure 4. Experimental apparatus showing fringe system on oscilloscope.

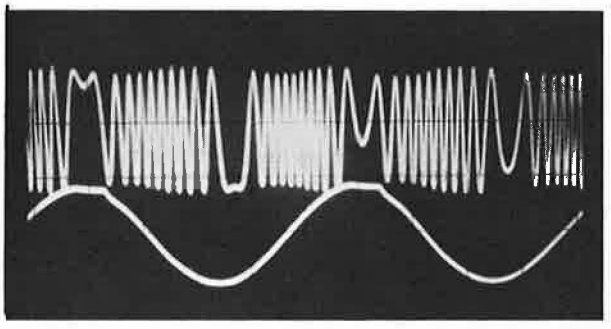

Figure 5. Interferometer output for a scotchlite target.

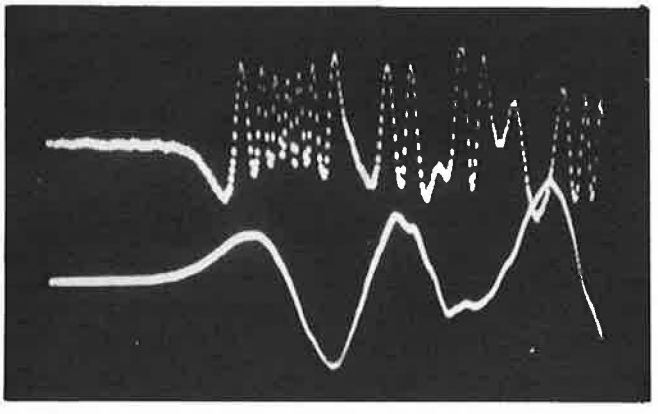

Figure 6. Interferometer output for a struck limestone block.

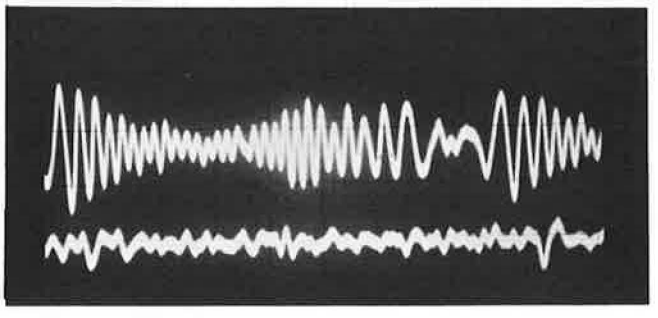

Figure 7. Interferometer output for anthracite coal sample.

$$\gamma = \frac{\sin(\omega_2 - \omega_1)T}{(\omega_2 - \omega_1)T} \tag{21}$$

The magnitude of the partial coherence factor, or $|\gamma|$, is a measure of the coherence of the 2 light beams whatever their origin. Thus we can compare 2 separate beams, parts of the same beam, or Doppler-shifted beams relative to stationary sources.

Detector Response Time and Maximum Particle Velocity

By using $|\gamma|$, we can determine the effect on coherence, or fringe visibility, as a function of response time. If all other sources of coherence degradation have been found acceptable and $|\gamma|$ is some number near unity, then an increase in T, the integration time in equation 21, will eventually cause $|\gamma|$ to reduce to a low value so that no fringes would be observed. If T is physically the response time of a given detector to the optical field being sampled, T must be as small as possible in order to have good fringe visibility. In particular, the argument of equation 21 must be small or $(\omega_2 - \omega_1)T < 1$. If $\omega_2 - \omega_1$ is the Doppler shift, then we evidently must have for a detector of given response time T

$$\Delta\omega(t) < 1/T \tag{22}$$

A typical photomultiplier may have an effective response time of about 10^{-6} sec; hence, measuring Doppler shifts $\omega_2 - \omega_1$ equal to about 1 MHz would be possible in principle. As a practical measure, in most of the measurements we performed, we employed solid-state detectors and amplifiers having considerably larger overall (combined) effective response times of about 10^{-5} sec. If a He-Ne laser is employed, this would mean that particle velocities as high as 3 cm/s could be detected.

Our principal reason for using solid-state detectors was that the cross terms in equations 5 or 14 could be enhanced by making A_o, the reference beam amplitude, very large. Such a procedure is possible by using solid-state detectors, but it cannot generally be used with a photomultiplier because of possible danger to the tube. In any case, the solid-state detectors and amplifiers that we used limited our peak particle velocities to about 3 cm/s. In the future, if the response times of these devices (plus amplifiers) are reduced, this peak particle velocity could be considerably increased.

Any other response time limitations imposed by any other piece of apparatus such as amplifiers, filters, and the like will have the same effect on the effect coherence or fringe visibility as a detector with poor response time will have.

Surface Properties

We do not intend to consider in detail the full range of surface properties to be encountered in actual situations; however, some simple general observations can be made that will tend to constrain what one can expect in any given situation.

Consider a perfectly diffuse surface. In such a case, the incident light flux F_o is scattered uniformly through a solid angle 2π. If the telescope aperture A is located at a distance R from this surface, the returned and collected light flux F_{ob} will be roughly

$$F_{ob} \approx \frac{A^2 r}{8R^2} F_o \tag{23}$$

where r = a surface reflectivity coefficient.

This simple formula shows clearly that the observed flux varies inversely as $1/R^2$ and directly with A^2, r, and F_o. One may compensate for low surface reflectivity by making F_o and A larger. However, a formula of this type is only valid when the particle size δ doing the scattering is less than S where S is the size of the focused spot

$$S \sim \frac{1.22\lambda R}{A} \tag{24}$$

In this case, because the diffraction-limited telescope of aperture A is used to both send and receive, S is limited by A. For very short observing distances, $A \sim R$ and $S \sim \lambda$, and the particular structure will not be resolvable when $\delta > \lambda$. Even if $\delta > \lambda$ but where $S > \delta$, we can still expect the surface to be diffuse. Whenever we have diffuse surfaces, the observed signal would be expected to drop as $1/R^2$. Such situations represent the poorest that could be encountered.

Note, however, that, for materials such as granites or other crystalline substances where crystal faces are frequently encountered, a drop-off considerably less than $1/R^2$ is to be expected under certain conditions. For example, consider a situation in which the diffraction limited spot size $S \lesssim \delta$, where δ represents the size of a highly reflective crystal face oriented perpendicularly to the axis of the incident light cone. In this special case, the observed flux could be much larger than that predicted by equation 22. It could be a large fraction of F_o. Materials of this type would not show the $1/R^2$ drop-off at least over distance ranges where $S \lesssim \delta$. It is interesting that behavior of just this sort has been observed in the laboratory for materials such as granite or hard coal where specular surfaces are frequently encountered. Anything that would be expected to enhance the specular characteristics of a surface (even an ordinarily diffuse one) thus would improve the returned signal. For example, one would expect that an improved signal would be possible in situations where surfaces are wet.

In actual experiments performed in our laboratory, we often found it necessary to search out the best point on a given surface. By moving the point of focus very slightly, one can always find these specular regions on most of the materials that we have examined. This thereby increases the signal-to-noise ratio dramatically. A more detailed account of tests on materials varying from scotchlite to soot and including various types of rocks is available elsewhere (3).

Insensitivity To Small Displacements

That piezoelectric devices are extremely sensitive to small relative displacements is well known. Typically, a particle displacement of 1 A° (0.1 nm), which is roughly the spacing in a crystal lattice, results in large signals. By comparison, the laser interferometer is a relatively insensitive device. To see this, we note that the He-Ne laser line has a wavelength of $\lambda = 6328$ A° ($\lambda = 632.8$ nm). For a system of the type discussed in this paper, measuring displacements much smaller than about 1 percent of a fringe spacing is unreasonable. Thus we cannot easily detect displacements of less than about $\delta \sim 0.01\ (\lambda/2) \sim 32$ A° [$\delta \sim 0.01\ (\lambda/2) \sim 3.2$ nm] even at low frequencies. This rough calculation makes it clear that the interferometer as currently envisioned will not compete in sensitivity with peizoelectric devices. However, when appropriate compensating sources such as small explosives are used, the lack of sensitivity of the interferometer need not pose a problem.

Miscellaneous

Many further minor difficulties stand in the way of obtaining good quality measurements having a simple interpretation. First, we note that problems of vibration, in some cases, may be serious because we are detecting relative line-of-sight motion.

If both the source and the interferometer are moving and the interferometer motion is unknown, inferring the source motion from the interferometer signal alone is not possible. In most cases dampening instrument motion considerably should be possible. We also note that observing times are typically short (in the millisecond range), and, unless the disturbance agitating the interferometer has a frequency in the kilocycle range, no vibration problems should occur. However, very low frequency measurements would not be immune to this problem. Nevertheless, in extremely noisy environments, some independent record of the acceleration of the interferometer could be kept, say, by the use of a piezoelectric transducer or another laser interferometric measurement by using the same laser. The interferometer motion could then be subtracted from the relative motion to get the true line-of-sight source motion. Finally, we reiterate that all motion detected by the interferometer is line-of-sight motion and anything that changes the line-of-sight distance contributes. Thus lateral motion makes a contribution. The fringes observed in this case are more characteristic of the surface roughness than they are of surface motion itself. Note also that such things as shear waves and pressure waves cannot be distinguished by their displacements alone.

Although limitations such as these are not to be dismissed lightly, they are not particularly significant for many problems in which one is primarily interested in scalar properties (not dependent on direction) of the surface motion. For example, if one is interested in measuring the scalar frequency amplitudes corresponding to any displacement source, the fact that both P and S waves are present is not particularly relevant because they have essentially the same time variation if they originate from the same source.

In situations where one is measuring the time of arrival of the signal, the onset of any motion whether line-of-sight, lateral, or P or S is all that is required. A wide variety of other scalar measurements, such as Q-values, relative stiffness, attenuation coefficients, and response characteristics, are essentially unaffected by the line-of-sight constraint. Therefore, even though this does place severe limits on problems in which highly directional vector properties, such as the direction of first motion, are desired, there remains a large class of practical problems that can be handled by this technique.

POSSIBLE APPLICATIONS

In this section, we outline several additional applications not already mentioned. Although, in most cases, only laboratory simulations of the experiments discussed here have been performed, we can draw some definite conclusions about the applicability of these techniques to various practical problems.

Although it has not been specifically discussed, the laser interferometer can easily be made portable because the laser and associated electronics may be operated on batteries. This situation ensures that field applications are realizable.

Mining Geophysics

Perhaps the first use in mining or tunneling situations of the techniques developed here would be in hazard detection. The roof fall and rock burst are 2 of the most frequent causes of mine fatalities. Either of them is usually preceded by distinct changes in the elastic properties of the rock that is ultimately to fail. Such changes can take the form of a change in the effective stiffness of a given structural member or a part of this member. For example, just before rock bursts in mine pillars, measured P-wave velocities through the pillar invariably are observed to increase from some anomalously low value to a more normal value (5). Behavior of this type can be monitored by doing a conventional P-wave survey with geophones or by using the laser interferometer. In certain situations in which time is critical, the simplicity and ease of operation of the interferometer could make it a convenient means of measuring such transient

phenomena before a disastrous failure.

The laser interferometer also could be used to detect loose slabs of rock by taking advantage of their reduced stiffness. A loose slab can easily be made to move through a larger displacement for a given applied force compared with nearby competent rock. Such increased displacements would appear as an increased fringe frequency.

The character of rock is often specified in terms of its Q-value, which, put simply, is inversely proportional to the energy loss per cycle that such a rock exhibits for a given acoustic input. Rock with a low Q-value is highly attenuating and generally has a low E-value. If rock of this type is struck by some impulsive source, it generally sounds dull because the high frequencies are more rapidly attenuated than the low frequencies are. On the other hand, rocks with high Q-values sound metallic when struck (even with nonmetallic objects or sources), and they tend to "ring" for a much longer time than the low-Q-value rocks. Rocks of this type have generally high E-values as well.

The laser interferometer could be used to rapidly obtain qualitative information on the Q-value of rock at or near the sampling point by merely ascertaining how long the rock or rock structure rings after being subjected to a given impulse. Roof rock in large rooms or rock in tunnel faces could be examined remotely by striking the near vicinity of the optically sampled point with a projectile and examining the response. A line of such measurements across the roof span or across an excavation face could then be used in principle to detect bad rock areas or zones. Such areas would be distinguished by having low Q-values or short ringing times compared with adjacent higher Q-value rock, which should have a higher Young's modulus and be more competent.

Apart from mining or tunneling applications of this type, there are situations in which techniques such as seismic holography are to be employed to image certain discontinuities on rock. Several techniques (including holographic techniques) that would, for example, attempt to look ahead of the working face in a tunneling operation have been contemplated by various investigators. The laser interferometer provides a simple remote means of rapidly obtaining the necessary arrival time data or other seismic data for such procedures provided sufficiently energetic impulsive seismic sources such as an explosive are employed.

Civil Engineering Applications

Perhaps the most interesting application that comes to mind in this area is the use of such a system in vibration analyses or modal studies of various structures. Information on the natural modes of vibration of existing buildings and bridges is essential if the integrity of structures in earthquakes or violent wind storms is to be ascertained. Such studies can be, and have been, performed by using contact transducers and the wind as a driving force; however, the laser interferometer would greatly simplify such measurements and, at the same time, give the experimenter great flexibility in his or her choice of measuring points.

Hostile Environments

Like holographic interferometry, the interferometric technique described in this paper could be applied to the examination of moving surfaces (or changes in indexes of refraction) in environments inaccessible to ordinary instruments because of high pressures or temperatures. The advantages of simple point measurement are that no holograms are required and that problems of interpretation of fringe data due to the problem of nonlocalized fringes do not occur. However, the holographic interferogram has the distinct advantage of covering an entire scene rather than a single point.

CONCLUSIONS

The experimental study presented indicates that a modified laser interferometer may

be employed to detect line-of-sight motion on unprepared rock surfaces at distances from the interferometer of at least 100 m. With further technical improvements in the system, improved signal-to-noise ratios and greater distances of operation are possible.

The demonstrated feasibility of the system for performing remote measurement of displacements on an unprepared nonspecular surface should provide considerable encouragement to those interested in improving and applying this technology to their own particular needs; in particular, there is reason to expect that such techniques might be used in tunneling and underground excavation in general for evaluating the integrity and safety of rock structures.

After this paper was prepared, the interferometer shown in Figure 4 was made portable (battery operated) and taken to a mine for tests. The tests are still in progress; however, results to date generally confirm the predicted usefulness of the interferometer in hazard-detection applications and rock-structure analysis in general. We have also recently begun construction of a folded beam design that uses high-quality, commercially available optics. This improvement promises to reduce significantly the size and weight of the system.

ACKNOWLEDGMENTS

We wish to thank R. Myers for his aid in designing a circuit for the solid-state detector. We also thank D. Dolinar for valuable discussion.

REFERENCES

1. G. L. Fitzpatrick, H. R. Nicholls, and R. D. Munson. An Experiment in Seismic Holography. U.S. Bureau of Mines, Rept. of Investigation 7607.
2. G. L. Fitzpatrick. First-Arrival Seismic Holograms. Acoustical Holography, Vol. 4.
3. R. A. Bruce and G. L. Fitzpatrick. Remote Vibration Measurement of Rough Surfaces by Laser Interferometry. U.S. Bureau of Mines, in press.
4. G. W. Stroke. An Introduction to Coherent Optics and Holography. Academic Press, New York, 1966.
5. W. Blake. Rock Burst Research at the Galena Mine, Wallace, Idaho, USA. U.S. Bureau of Mines, Technical Progress Rept. 39, 1971.

MICROSONIC DETECTION OF LANDSLIDES

Marvin L. McCauley, California Department of Transportation

The microsonic activity (subaudible rock noise) that is recorded in a material can be used to evaluate the stability of slopes in the area. The method can be used in conjunction with other monitoring devices for more thorough monitoring of slope stability. The California Department of Transportation, through a series of research studies, has shown the feasibility of the technique. Currently, the method is used to provide information on activity of landslides, stability of cut slopes, and effectiveness of field corrections for stability problems. Several case histories illustrate uses of microsonic monitoring. The Porto Marina landslide was monitored to minimize the hazard and inconvenience to traffic on Calif-1. Monitoring of the Thornton Bluffs landslide illustrates the relationship of microsonic activity, slope indicators, and nail measurements. Newly constructed cut slopes have been monitored to determine potential for slope failures. Corrective measures for the American Canyon landslide were monitored to evaluate their effectiveness.

•THE California Department of Transportation is using subaudible rock noise (SARN) to monitor various types of slope stability problems. This technique together with other methods, such as use of slope indicators, measurement across cracks, and surveying of points, is available for monitoring. Each slope stability problem must be considered carefully to determine which monitoring method or combination of methods is most suitable. The case histories described in this paper illustrate some of the benefits that can be derived from SARN monitoring.

Interest by the department in the use of SARN to monitor the stability of slopes developed in 1962. A study by the University of California (1) that was done for the Transportation Laboratory of the department concluded that actively moving landslides generate subaudible rock noise and that equipment capable of detecting and recording these noises was available. These noises have been referred to as microsonic noises, acoustic emission, microseismic noises, and subaudible rock noise. The second phase of the department's investigation of SARN evaluated the practicality of using SARN recordings to monitor slope stability. Four conclusions were drawn from this study (2).

1. SARN rate reflects the stability of the immediate area.
2. Number of counts increases as stability decreases.
3. SARN rates should be considered as relative values rather than absolute numbers. Changes in SARN rates are significant for evaluating slope stability.
4. Improvement in equipment and field techniques was needed.

Subsequent study by the Transportation Laboratory has evaluated equipment for detecting and recording SARN and has modified the field techniques. The conclusions and recommendations contained in the final research report are as follows (3):

> The experience gained through equipment development and the data observed and analyzed both in the case histories included with this report and in ongoing projects indicate that subaudible rock noise (SARN) is directly related to instability.
>
> SARN rates do not appear to be absolute measurements of activity but rather provide a qualitative evaluation of stability, i.e., increases or decreases in SARN rates reflect decreases or increases in stability.

Given a site history and a SARN rate indicative of stability for the site, properly trained personnel can evaluate site stability by monitoring, and give a subjective decision as to the probability of failure at some time following the monitoring.

There is evidence that stability changes can be detected by SARN monitoring up to several weeks in advance of other forms of monitoring. Additional experience with this phenomenon should lead to further applications of SARN monitoring.

Care must be exercised in selecting and training personnel to make such evaluations. Proper equipment for monitoring is also mandatory.

Based on the experience and knowledge gained during this research, further use of SARN monitoring as a means of slope stability evaluation is recommended. Because these decisions are subjective rather than absolute, it is also recommended that only experienced personnel be utilized for stability evaluations.

As a result of experience gained while monitoring various slope stability problems, a mobile SARN laboratory has been built to improve on-site monitoring capability.

The case histories in this paper in which SARN has been used were chosen because they illustrate the more common applications to slope stability problems and because data obtained on these cases provide information about the capabilities of SARN as a monitoring technique.

MONITORING LANDSLIDES

Porto Marina Landslide

A slope above Calif-1 along the coast near Los Angeles began to fail in 1969. A report by Mearns (4) indicated that unusually heavy rains had preceded the developing failure. By the time the SARN monitoring crew arrived at the site, the slope was unstable and falling material had blocked 1 lane of the 4-lane highway. A large cantilevered house (Figure 1) was starting to slide toward the road. The traffic count at the time was 30,000 cars/day, and no good alternate route was available. The SARN monitoring was to be used to evaluate the stability of the slope and to minimize the hazard and the inconvenience to traffic using Calif-1. Monitoring began at 11:00 a.m. on February 20, 1969, and was described as follows by Mearns (4).

The first noise counts, although high, did not suggest imminent failure. However, at 1300 hours the count abruptly jumped to a dangerous level. Because of the extremely high noise count and measurable movement of up to ½ inch (12.7 mm.) across cracks in the driveway, District 07 maintenance personnel controlling traffic on the road below were told that the slope was considered dangerous. At 1352 hours they ordered Road 07-LA-1 closed as a safety measure.

Noise rate continued at a serious level until approximately 1600 hours on February 20, 1969. At approximately 1430 the noise was nearly continuous and a count was difficult to obtain. By 1700 hours the noise rate had dropped back to the pre-movement level. During this time period severe wrenching of the house occurred, most of the glass broke out and three of the front five caissons separated completely from the house and a fourth was badly damaged. No surveyed measurements were taken of this movement, however, the taped distance between one microphone location and the uppermost crack at the head of the slide increased from 18 to 23 feet (5.5 to 7 m.) and the elevation dropped nearly four feet (1.2 m.) with respect to the sewer line at the head of the slide.

At the toe of the slide small slumps of soil and rock occurred during the entire period of high activity. Also during this period, boulders of sheared material as large as 6 feet (1.8 m.) in diameter rolled down the slope and out as far as centerline of the highway. A few smaller fragments rolled across centerline.

The noise rate continued to decrease after 1700 hours and at approximately 2100 hours maintenance personnel were notified that the noise rate was at a nonhazardous level and the standby cleanup crew was sent home.

Monitoring was continued through 1600 hours on February 21, 1969, with no signs of increased activity and maintenance personnel were required only to keep people out of the hazardous area.

As heavy equipment for demolishing the house was moved into the area and began work, the noise rate jumped to the original noise level of February 20, 1969 and tape recordings were again

started. These recordings were continued until the last microphone connection was broken by the work (approximately 2000 hours). At no time during the destruction of the house did the noise rate reach a hazardous level.

A plot of SARN counts per minute against time is shown in Figure 2. The high SARN rates correspond to the most intense slide activity. This plot also provides a way of determining whether the SARN rates are increasing or decreasing. This type of information was extremely useful for deciding when to close and when to open the road.

Thornton Bluffs

A coastal area just south of San Francisco is subject to continuing erosion by the ocean. The bluffs, composed of poorly consolidated sands, silts, and clays, contain numerous slides. One of the slides overhangs an abandoned state highway right-of-way (Figure 3). The upper scarp traverses a subdivision cul-de-sac and affects several houses (Figure 4).

Several types of monitoring were applied to this site. In addition to SARN listening, slope indicators were read, and measurements across cracks in the cul-de-sac were made regularly. The monitoring provided information on the configuration and rate of movement of the slide and helped evaluate the hazard to residents of the area.

Plots of the results of 3 different types of monitoring are shown in Figure 5. This figure illustrates the correlation of the different monitoring techniques. In this particular case, increased SARN activity was noted in December 1973; increased rate of movement for the other monitoring was noted about 2 months later. In some cases, SARN appeared to indicate a change in stability earlier than some other monitoring systems.

MONITORING CUT SLOPES

Pacheco Pass

The first evaluation by the Transportation Laboratory of the use of SARN to monitor new cut slopes has been reported previously (3). Several slides had occurred on a highway relocation project in the Central Coast Ranges of California. As a result of these stability problems in the fractured and sheared sandstone and shale encountered on the project, several cut slopes were selected for SARN monitoring. Figure 6 shows the relationship between SARN rates and site conditions such as construction activity, rainfall, and a local slide. The highest count was obtained shortly after the slide had occurred. Figure 7 shows the local slide that occurred. The monitoring location was near the man standing beside the highway. The results of this study were encouraging enough to warrant further monitoring of cut slopes with the SARN method.

Anderson Grade

The construction of a segment of I-5 in the Klamath Mountains of northern California was complicated by difficult alignment problems imposed by the rugged terrain. Five cuts over 100 ft (30.5 m) high had been designed in fractured and sheared, fine-grained metamorphic rock. The cut-slope angles would be steep, and presplit blasting would be required for some of the slopes to minimize the disturbance of the rock remaining in the cut face. SARN monitoring was begun in March of 1968 before construction. During construction, the slopes were monitored at approximately 1-month intervals. Monitoring was continued for several months after completion of the construction. SARN rates were low throughout the period of monitoring. No major slope failures occurred on any of the monitored slopes.

Figure 1. Porto Marina landslide.

Figure 2. Subaudible rock noise counts recorded at a location in the Porto Marina landslide.

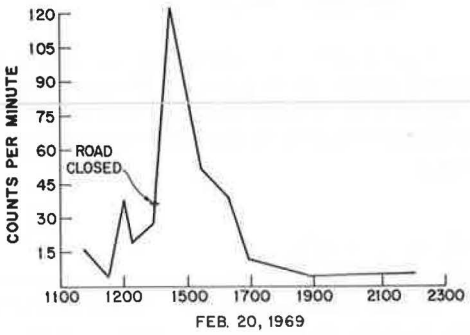

Figure 3. Thornton Bluffs landslide.

MONITORING CORRECTIVE WORK IN AMERICAN CANYON

In 1968, during the construction of I-80, a large landslide developed in soft sedimentary rocks. The slide was located several miles (kilometers) northeast of Vallejo, California, and is referred to as the American Canyon slide. Initial efforts to correct the slide were not successful, and, in early 1969, SARN monitoring of the slide was begun.

Figure 4. Cracks in a cul-de-sac at head of Thornton Bluffs landslide.

Figure 5. Subaudible rock noise counts, nail point measurements, and slope indicator measurements taken at head of Thornton Bluffs landslide.

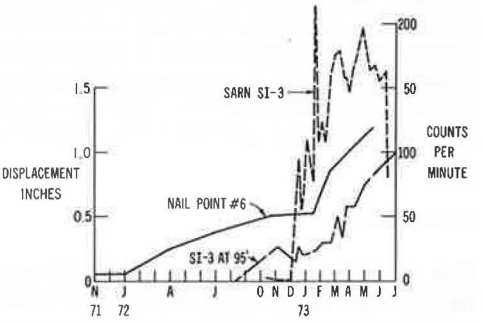

Figure 6. Subaudible rock noise counts recorded at station 46 near Pacheco Pass.

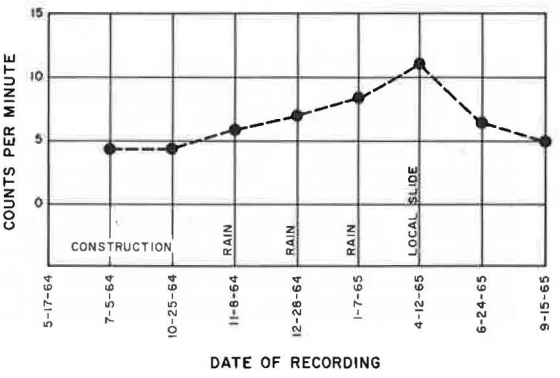

Figure 7. Small slide in cut slope at station 46 near Pacheco Pass.

Figure 8. Subaudible rock noise counts recorded at station 483 in American Canyon.

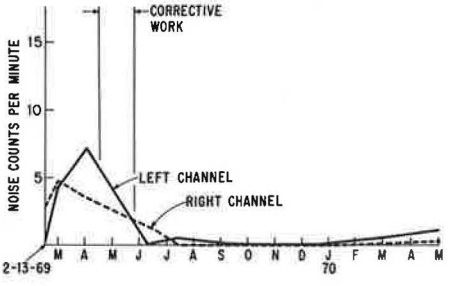

Additional work to correct the slide included the installation of a series of 600- to 800-ft-long (183- to 244-m-long) horizontal drains to remove groundwater and the removal of 350,000 yd^3 (267 759 m^3) of material from the upper part of the slide. The SARN counts that were recorded at station 483 are shown in Figure 8. The SARN rate dropped steadily during the corrective work and remained low after the correction. This illustrates how SARN monitoring can be used to monitor the effectiveness of correction measures that are used on a slope stability problem. Left channel and right channel in Figure 8 refer to 2 separate microphones that were installed adjacent to each other and operated simultaneously. The correlation between the 2 records increases the confidence that can be placed in the SARN rates.

SUMMARY

The case histories presented in this paper illustrate some of the uses that the California Department of Transportation has made of SARN monitoring. The method has provided useful information about the activity of landslides, the stability of cut slopes, and the effectiveness of corrective measures that are applied to slope stability problems.

REFERENCES

1. R. E. Goodman and W. Blake. Microseismic Detection of Potential Earth Slumps and Rock Slides. College of Engineering, Univ. of California, Berkeley, Final Rept. SA MR 128, July 17, 1964.
2. M. L. McCauley. The Use of Sub-Audible Rock Noise (SARN) Recordings to Monitor Slope Stability. Engineering Geology Bulletin, Vol. 2, No. 2, July 1965, pp. 1-8.
3. R. Mearns and T. Hoover. Sub-Audible Rock Noise (SARN) as a Measure of Slope Stability. Transportation Laboratory, California Department of Transportation, Research Rept. CA-DOT-TL-2537-1-73-24, Aug. 1973.
4. R. Mearns. Sub-Audible Rock Noise in Random Samples. Materials and Research Department, California Division of Highways, May-June 1969, pp. 1-7.

EVALUATION OF GEOPHYSICAL SYSTEMS FOR REMOTE SENSING OF SUBSURFACE CAVITIES IN KANSAS

James W. Spencer, Jr.,* Chevron Oil Field Research Company, La Habra, California; and
James F. Koca, Harold T. Rib, and Craig P. Falls,** Federal Highway Administration

The Federal Highway Administration and its contractors, in cooperation with the State Highway Commission of Kansas (now the Kansas Department of Transportation), completed a field program in Kansas during 1971 to evaluate field geophysical systems for detecting subsurface cavities. The geophysical systems included passive microwave radiometers, an impulse radar profiling instrument, and direct-current electrical resistivity. Verification borings were completed in 1972 after analysis of the field data. Field data and test borings are presented for 1 traverse line in Galena, Kansas, to characterize the research findings. Passive microwave radiometers are sensitive to soil moisture and often record the effects of surface drainage, groundwater seepage, and subtle topography. The penetration of microwaves into soils, however, is limited, and the microwave radiometers are not well suited for detecting subsurface cavities. The impulse radar profiling system produced a graphical output that closely approximated the subsurface soil, rock, water, and void interfaces. The depth of radar penetration was limited to 8 ft (2.4 m) because of the presence of moist, clay-rich soils. Electrical resistivity proved to be the most useful technique for delineating subsurface materials. Geoelectrical soundings are well suited for locating conductive and insulative layers, but, because of the principle of equivalence, they may be unable to distinguish a water-filled cavity from another conductive subsurface zone.

•SERIOUS problems are encountered in the construction and maintenance of highways in areas with subsurface openings. The ceiling rock over the opening may collapse under heavy construction equipment, and the completed highway will be susceptible to subsidence. Whether the openings result from solution of natural earth materials or various mining activities, detection of the openings during the planning stage of highway construction currently is largely an expensive hit-or-miss drilling procedure. The problem of detecting subsurface cavities, therefore, was included for study under Project 4E of the Federally Coordinated Program of Research and Development in Highway Transportation (FCP) being conducted by the Federal Highway Administration (FHWA). A coordinated research effort by the FHWA, FHWA contractors, and state highway and transportation departments was formulated to investigate aerial remote sensing and field geophysical systems for detecting subsurface openings. The first test area investigated was in Kansas. A cooperative effort between the Federal Highway Administration and the State Highway Commission of Kansas (now the Kansas Department of Transportation) took place in which both aerial remote sensing and field geophysical systems were evaluated. The results of the evaluation of both the aerial and geophysical systems are published in FHWA staff reports (1, 2). This paper describes the results obtained for one of the field test sites. Three geophysical systems were evaluated at this site.

*Mr. Spencer was with the Federal Highway Administration when this research was performed.

**Deceased.

Figure 1. Four field test sites in eastern Kansas.

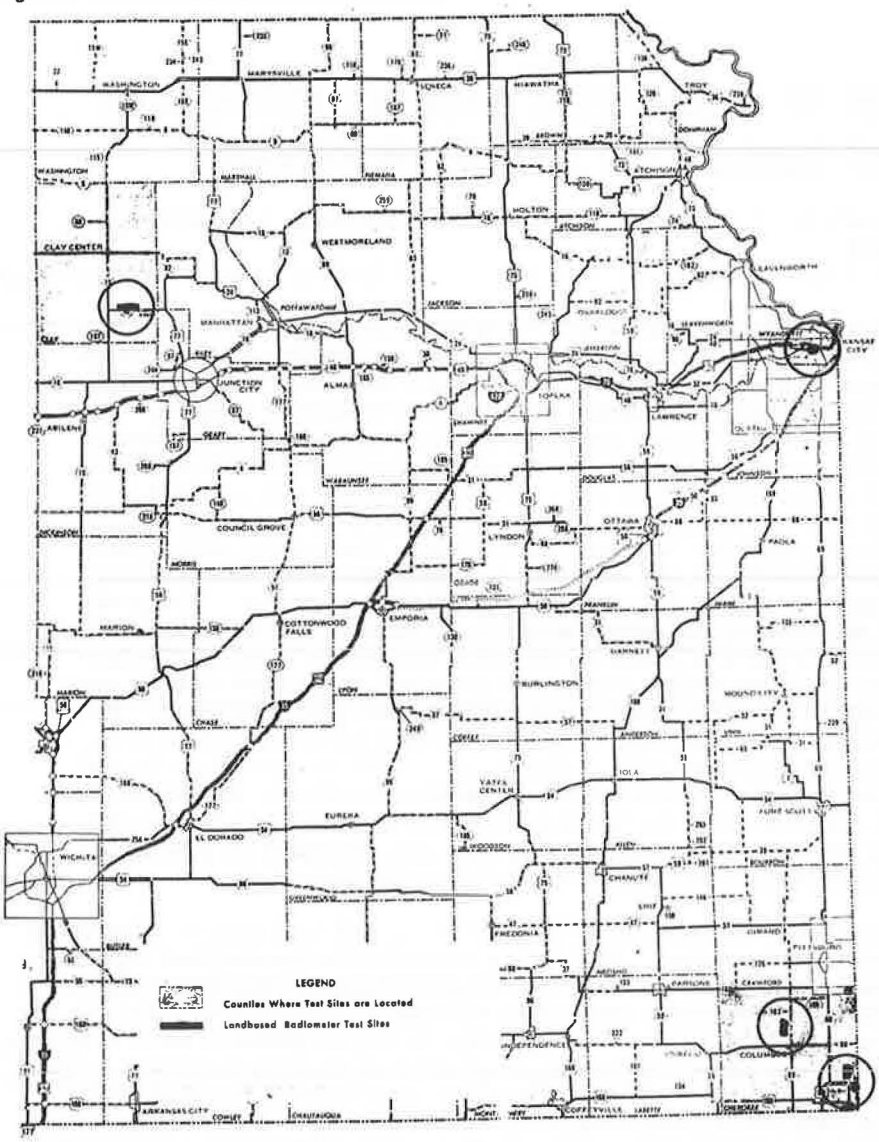

FIELD PROGRAM

The State Highway Commission of Kansas suggested possible test sites in Kansas for the field program. Test sites and traverse lines were selected in July 1971 by the commission, FHWA personnel, representatives of the contractor, and their subcontractor. Figure 1 shows the 4 test sites in eastern Kansas: (a) shaft mines in a zone of lead and zinc mineralization in Galena, Kansas; (b) shaft mines in a coal seam near Scammon, Kansas; (c) subsurface solution of a limestone stratum in Clay County, Kansas; and (d) subsurface limestone mine in Kansas City, Kansas, that had been a test site during the initial aerial program.

The geophysical surveys were conducted in August 1971. Highway commission personnel surveyed and staked the traverse lines and obtained soil moisture, temperature, and density measurements at selected stations. Passive microwave surveys and im-

pulse radar profiling surveys were performed. Electrical resistivity surveys were conducted during the field surveys. Each geophysical system was evaluated at the Galena and Scammon test sites; only microwave and limited resistivity data were acquired at the Clay County and Kansas City test sites. The geophysical surveys were analyzed by the investigators (3, 4) and a comparative analysis of the data was performed by FHWA staff. To verify the analysis of the data, FHWA directed the placement of borings over selected points at the Galena and Scammon test sites. The borings were accomplished in August and September 1972 by the highway commission.

This report presents the geophysical data for 1 survey line in Galena, Kansas. Galena lies in the tri-state zinc-lead district of Missouri, Oklahoma, and Kansas. Mississippian strata of limestone, chert, dolomite, and shale occupy nearly horizontal positions; sphalerite and galena are the principal ore minerals. Ore deposits are found only where structural deformation or solution and subsequent slumpage in the limestone strata created favorable premineralization reservoirs. Brichta and Ryan (5) conducted extensive electrical resistivity surveys in an area immediately north of Galena. Their work provides representative values for the resistivity of different geological formations. Cook and Van Nostrand (6) developed the theory for interpreting resistivity data over the shale-filled sinkholes in the tri-state area. Van Nostrand and Cook (7) included numerous examples comparing interpreted resistivity data from the tri-state area to borehole information by Brichta and Ryan (5).

An aerial mosaic of Galena (Figure 2) shows that much of the ground surface has been disturbed by mining operations, and fill material of either cobble-sized or finely crushed chert covers most of the field area. Survey lines Galena A and C were established where the ground surface was apparently undisturbed and covered by a minimal amount of fill material and vegetation. It would have been desirable for the survey to cross known subsurface openings, but published (8) and unpublished maps were insufficient for determining their exact location. Survey lines were selected to pass near open shafts and collapsed areas and thus hopefully over target subsurface openings. For example, the Galena A traverse (Figure 2) was selected to pass over mapped mine workings between stations 19+10 and 20+30. In addition, a large area of ceiling rock had collapsed adjacent to this survey line at station 19+65. The large collapsed area on Galena A is shown in Figure 3.

GEOPHYSICAL SYSTEMS

Passive Microwave Radiometers

Passive microwave radiometer measurements were obtained with a microwave field laboratory (Figure 4). Dually polarized radiometers with observational wavelengths of 21, 6.0, 2.2, and 0.81 cm are mounted on a hydraulically operated boom. Continuous microwave measurements were taken as the heavy field laboratory was driven forward and backward along each traverse line. Microwave profiles were obtained at 15, 30, and 45 deg above nadir for each traverse line. Aluminum foil strips were placed at discrete control stations to mark the radiometric data with respect to traverse position.

The energy received by a passive microwave radiometer, referred to as the brightness temperature, is the sum of energy emitted from the terrain surface plus the reflected sky energy. At microwave wavelengths, the differences between the radiometric brightness temperatures of various terrain surfaces are primarily the result of differences in their emittances, and variations in temperature are less important. For example, a smooth water surface has an emittance of 0.05 at 1.5 GHz and 0.3 at 70 GHz and will always appear very cold; soils and bedrock have emittances between 0.8 and 0.95 and will appear warm. The microwave brightness temperatures are dependent on the physical properties of the earth material, including moisture content; roughness of the surface at the observational wavelength due to microrelief, soil particles, or vegetative cover; and layering in the material. Compositional changes in a soil are of minor importance; only small effects are due to increased adsorption of water on clay particles.

The emission of microwaves from a smooth terrain surface without vegetative cover

Figure 2. Galena, Kansas, survey lines.

Figure 3. Collapsed ceiling rock over mine adjacent to survey line.

is primarily determined by the material's dielectric constant. Lundien (9) studied the electromagnetic propagation constants of soils between 1.0 and 1.5 GHz—a spectral band that includes the 21-cm radiometer. A strong correlation was noted between the dielectric constant and the volumetric water constant of a soil. This relation is one that is nearly independent of type of soil. Soils have a relative dielectric constant of approximately 3 when oven dried, and this value increases uniformly with moisture content to approximately 81, which is the dielectric constant for water. This relationship between the volumetric water and the dielectric constant, which determines the surface emittance, enables one to map soil moisture content in terms of brightness temperatures. In addition, clays commonly have a higher volumetric water content than either sands or silts at the same capillary pressure; therefore, brightness temperatures may grossly delineate the texture of adjacent soil units. The depth of microwave penetration into soils is correspondingly very sensitive to increases in soil moisture content, and microwave penetration is severely limited in all but the driest natural conditions. Penetration is reduced further in clay soils because clays have higher loss tangents than other soils have at the same volumetric water content. In Galena, the effective penetration of the longest wavelength (21 cm) radiometer was probably always less than 3 ft (0.91 m).

Although the reflectance of a smooth surface is determined by electrical properties of the material, the reflectance will decrease as the surface becomes increasingly rough and each irregularity approaches the condition of a blackbody. A diffusely rough surface, such as vegetation, has microwave emittances near unity such that the recorded brightness temperatures are nearly independent of the observation angle and the actual physical properties of the earth materials.

As microwaves travel through a material, they are partially reflected whenever they encounter a change in dielectric constant or electrical resistivity. For a uniformly layered material, the subsurface reflections would combine with surface reflections to produce interference effects, depending on the thicknesses of the layers, their electrical properties, and the wavelength of the transmitted signal. However, because of the variability of soil properties and layer thicknesses, there will be no simple relation between the brightness temperature and the presence of a subsurface opening or even water table. Moreover, the penetration of microwaves is sufficiently limited in all natural earth materials that primary detection of a subsurface opening is probably impossible. The only physical basis for operating a microwave survey to detect subsurface openings is that soil moisture in the overburden may reflect the presence of an air- or water-filled opening.

Impulse Radar Profiler

An impulse radar system, known as electromagnetic subsurface profiling (ESP), that can be considered as an electrical analogue to seismic reflection profiling has been developed (Figure 5). It can detect, record, and graphically display dielectric interfaces below the ground surface. The radar pulses are transmitted into the ground by a small transmitter-receiver sled that is towed across the ground at a velocity of 1 to 2 mph (1.6 to 3.2 km/h) by a 4-wheel-drive vehicle or by hand in rough terrain. The pulse is partially reflected as it encounters an interface of materials with different complex dielectric constants, and the reflected pulses from successive material interfaces add vectorially in the time domain to produce an analogue signal. The analogue signals are first recorded on magnetic tape at a sampling rate of 4 to 6 points/ft (13.2 to 19.8 points/m) of traverse line. The magnetic tape can be outputted on a graphical recorder in the field vehicle to enable field sampling of subsurface interfaces. The analogue tape can finally be computer processed to enhance or suppress reflections from interfaces at specific depths of interest.

Electrical Resistivity

Constant depth resistivity traverses and geoelectrical sounding by means of the Wenner

Figure 4. Microwave field laboratory in Galena, Kansas.

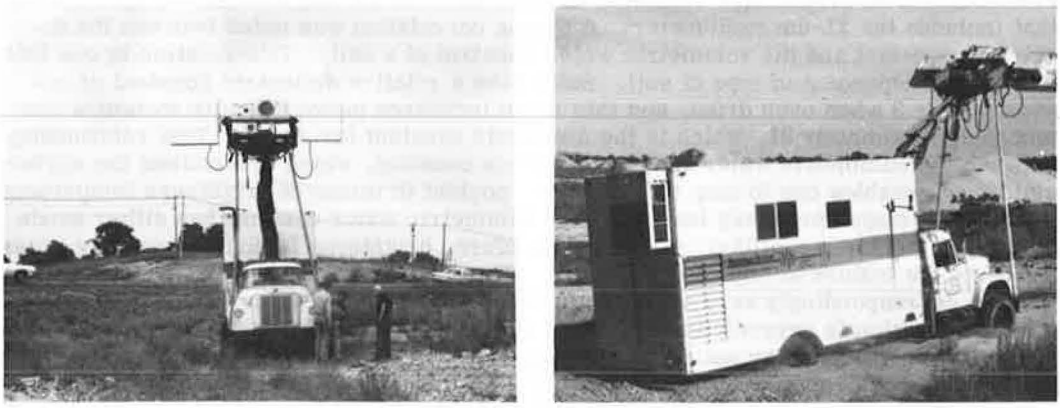

Figure 5. Vehicle and sled and impulse radar profiler.

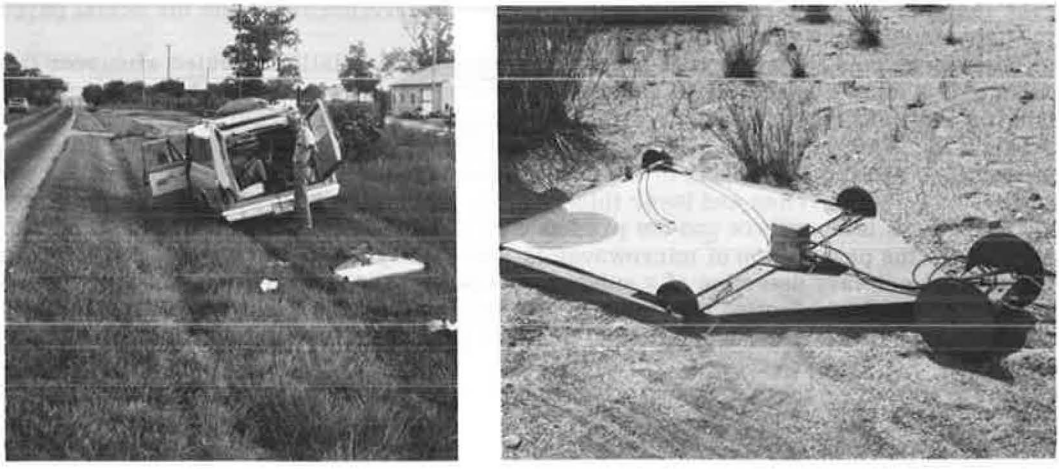

configuration were conducted over suspected subsurface cavities at each test site. The direct-current instrument ran off dry cells and employed copper sulfate porous pots for potential electrodes. An initial field analysis of the data, based on an empirical method of interpretation (10), facilitated the collection of complete and relevant data. It was found, however, that empirical approaches were insufficient for the complex conditions encountered in Kansas where there were large resistivity contrasts between adjacent zones and subsurface layers. All the electrical soundings in this study were interpreted by using theoretical master curves (11). The interpretation of constant depth resistivity traverses was facilitated by comparison with theoretical curves (7) for traverses across vertical dikes and buried, tabular conductors or insulators.

ANALYSIS OF GEOPHYSICAL DATA

Passive microwave traverses, a radar profiling survey, a constant depth resistivity traverse, and 9 geoelectrical soundings were conducted along survey line Galena A (Figure 6).

Passive Microwave Radiometers

The microwave brightness temperature curves shown in Figure 6 are for the 21-cm wavelength and 30-deg viewing angle traverse. No significant differences were noted between the horizontally and vertically polarized microwave plots. The traverses found low brightness temperatures, which is a pattern that might be expected for cavities between stations 12+70 and 13+30, 16+70 and 18+30, and 18+70 and 19+40. The anomaly between stations 12+70 and 13+30 was traced to a black, mucky clay that lies near the surface and rutted easily during vehicle traverses. The subcontractor (4) attributed the large, broad microwave cool area between stations 16+70 and 18+30 to a sharp increase in material density. Instead, there appears to be groundwater seepage in this area. The evidence is a strip of heavy grass and small trees adjacent to the survey line and extending between the same survey stations. The microwave anomaly between stations 18+70 and 19+40 is centered about station 19+15, which lies within an area of mapped mine workings (8). We can examine the anomaly between stations 18+70 and 19+40 as a possible extension of the mine workings.

Impulse Radar Profiler

After analyzing the enhanced radar profile for Galena A, the contractor suggested 8 locations where borings would presumably find subsurface voids less than 8 ft (2.4 m) below the surface (3). These recommended boring sites are indicated by arrows above the interpreted soil-rock profile at the bottom of Figure 6. The radar patterns for 2 of the potential sites (at stations 18+65 and 19+10) are shown in Figure 7. These anomalous patterns were similar to those obtained over known cavities.

The impulse radar profiler records reflections from dielectric interfaces that could be voids or the related fractures that can propagate into the ceiling rock. They also could simply be contacts between earth materials, such as slumpage materials or filled areas, that have different complex dielectric constants. Thus, full interpretation of the radar profiles was delayed until the geophysical data were analyzed. In the final analysis, several dielectric interfaces did correlate with features such as shale-filled slumps, filled areas, or near-surface bedrock.

Constant Depth Resistivity Traverse

Certain geological information can be extracted directly from the constant depth traverse (Figure 6). For other stations, the traverse provides information useful in the interpretation of electrical soundings. The most notable feature of the traverse is the symmetrical rise in apparent resistivity centered around station 15+70. Inspection of theoretical curves for a Wenner configuration traverse across a vertical contact indicates that there must be a more resistive material that can be modeled as a vertical dike in the subsurface between stations 14+50 and 16+70. The W-shaped traverse between stations 11+80 and 13+50 probably indicates a resistive material that is closer to the surface under station 12+70. The unusual peak in apparent resistivity at station 19+25 occurred because the current electrode was directly opposite the large collapsed area shown in Figure 3. The peak in apparent resistivity does not represent a resistive, subsurface material under station 19+25.

Geological Soundings

Nine geoelectrical soundings, or depth tests, were performed along line Galena A. Large resistivity contrasts occurred between adjacent subsurface layers. The dry, crushed chert overburden had resistivities of approximately 1000 Ω•m; the underlying chert bedrock had values of approximately 500 Ω•m; and the conductive slump or fill materials at intermediate depths had values near 75 Ω•m. The weathered rock layers

Figure 6. Geophysical data and interpreted soil-rock profile for survey line Galena A.

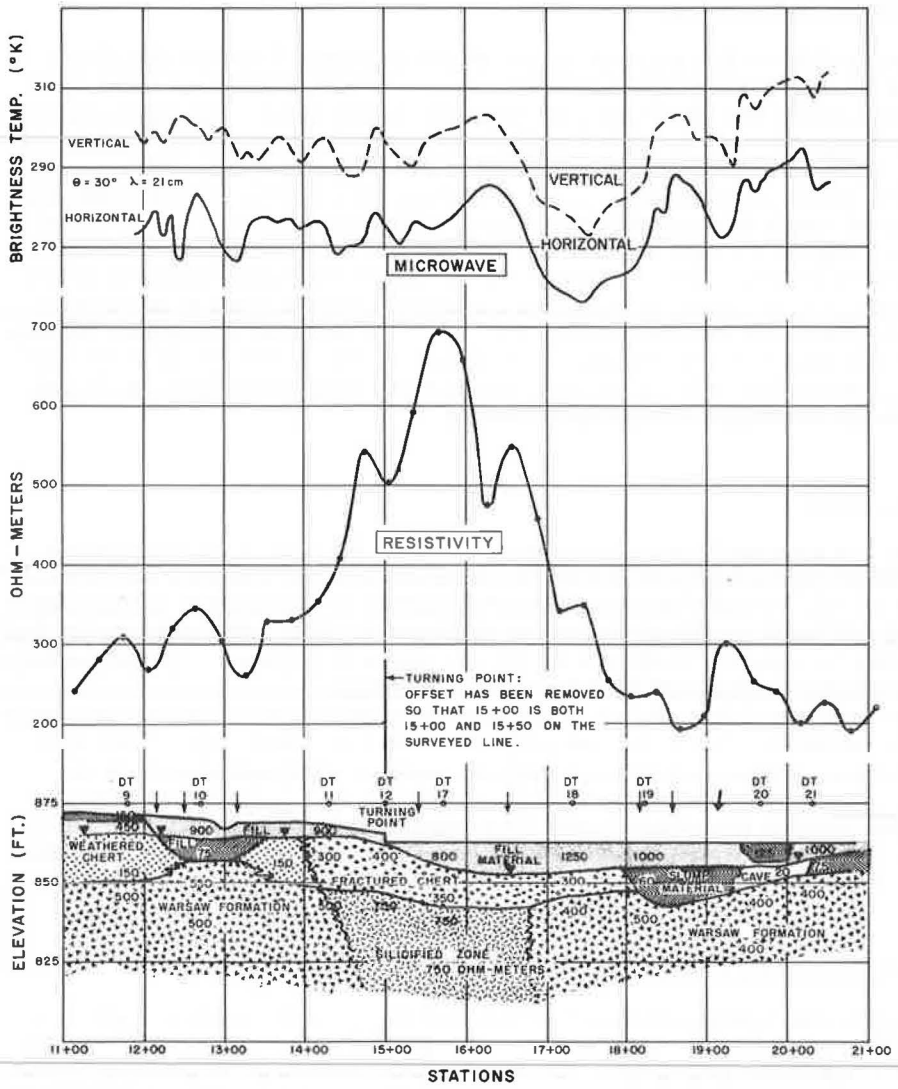

Figure 7. Enhanced radar profile indicating location of possible cavities along a portion of survey line Galena A.

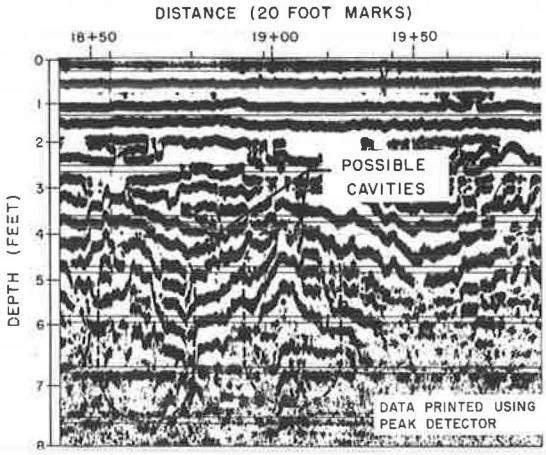

had lower resistivities than the parent rock. Detailed curves are included in the FHWA report (2). Distinguishing the conductive earth materials from possible water-filled openings is difficult. To do so requires a detailed consideration of the principle of equivalence in geoelectrical prospecting (12), and distinguishing the materials may finally be impossible even though their resistances are different. This uncertainty occurs because, for certain relations of the parameters of a 3-layer geological section, changes in the resistivity and thickness of the middle layer do not produce noticeable changes in the electrical sounding curve. In the case of a conductive middle layer, increasing or decreasing the thickness and resistance of the intermediate layer by a multiplicative factor is possible, within certain critical limits given by Pylaev's nomograms (12), without changing the measured field curve. A thin, water-filled cavity thus can be electrically equivalent to a thicker, more resistive layer of fill, and only geological reasoning can help to resolve the uncertainty. For example, the interpreted electrical sounding at station 12+70 indicated the possibility of a fill material with a thickness of 9 ft (2.74 m) and resistivity of 75 Ω·m or the possibility of an extensive, excellent conductor (water-filled opening) at a depth of 5 ft (1.5 m). This latter condition was geologically improbable at this location; therefore, a layer of fill was interpreted to overlie an old erosional surface on the chert bedrock. This interpretation also explains the W-shaped constant depth traverse across this area.

The presence of a subsurface void was suggested near station 15+40. However, analysis of electrical depth tests 12 and 17 indicated the presence of a resistive material at a shallow depth. The constant depth traverse similarly indicated the presence of a high resistivity material in the form of a vertical dike through this section. This harder material was interpreted to be chert, which is evident as outcrops at an offset to stations 16+00 and 16+20.

Electrical depth test 20 (station 19+65) was completed adjacent to the area of the collapsed ceiling rock (Figure 3) and indicated a conductive intermediate layer which, from ground observation, was identified as the water-filled opening. A conductive surface layer, with a surface expression of tall grass and moss ground cover, was located over the water-filled opening. A conductive intermediate layer also was indicated by depth test 19 at station 18+20. This raised the question of whether the cavity extended to this station or whether slump material was present. The radar and microwave anomalies in this region indicated the possibility of the extension of the water-filled cavity from station 19+10 to station 18+20, but the lateral contact between slump material and the water-filled opening could not be defined.

COMBINED ANALYSIS AND BORING RESULTS

A combined analysis of the constant depth traverse and electrical sounding 10 suggested that an area of fill is between stations 12+00 and 13+50. It was reasonable for the radar profiling anomalies at stations 12+15, 12+50, and 13+15 to be dielectric interfaces within the fill or at the contact of the fill with the old ground surface. A shallow hole was augered at station 13+15 to test this interpretation. Chert gravel with a clay matrix was found to a depth of 5.3 ft (1.6 m) where there was a transition to practically clay-free chert gravel. An electromagnetic pulse experiences the same phase shift when it passes from clay-rich to clay-free material as it would passing from soil to an air-filled void. The transition in clay content was probably the interface that had been interpreted as a void. The fill material continued to a depth of 8.8 ft (2.7 m) where chert bedrock was encountered.

An analysis of electrical soundings 12 and 17 suggested that fractured and then probably massive chert should be near the surface at station 15+40, a location where the radar profiling unit found a subsurface dielectric interface. The constant depth traverse indicated that the massive chert should extend between stations 14+50 and 16+70. A shallow test hole was drilled at station 15+30, and this hole verified the presence of first fractured and then massive chert below a depth of 3.2 ft (0.97 m).

The large microwave cool area between stations 16+40 and 18+30 is believed to be due to groundwater seepage, and the dielectric interface at station 16+50 could be either

groundwater or the near-surface chert. The smaller microwave cool area between stations 18+70 and 19+40 could reflect an extension of the mine workings that were mapped between stations 19+10 and 20+30, and, because of the principle of equivalence, the electrical sounding at station 18+20 could not verify or disprove this hypothesis. The warm microwave temperatures between stations 19+40 and 20+15 could have resulted from the tall grass between these stations and cannot be interpreted as either the presence or absence of a subsurface water-filled opening. A drill hole was completed at station 18+80 to test whether the microwave radiometer had delineated an extension of the mapped cavity. The boring found clay-free chert cobbles to a depth of 6.6 ft (2 m) and then clay-bound chert with minor amounts of limestone to 19.3 ft (5.9 m) where chert bedrock was encountered. The drill had found slump material and not an extension of the mining activity.

CONCLUSIONS

This report describes the analyses of 3 geophysical systems for detecting subsurface cavities for test line Galena A. Additional surveys were performed in the Galena area as well as in 3 other test areas. The conclusions are based on the analysis of data from all the test sites as reported in the FHWA staff report (2).

The penetration of microwaves is sufficiently limited in all natural earth materials so that primary detection of a subsurface opening is probably impossible with a passive microwave radiometer. Near-surface soil moisture content may occasionally reflect the presence of an air- or water-filled subsurface opening. However, this physical basis of operation is tenuous and is easily disrupted by the effects of surface drainage, groundwater seepage, and subtle changes in topography. The operational requirement of a ground surface that is smooth at the observational wavelength is an additional restriction in areas with natural, vegetative cover. Passive microwave radiometers are not well suited for detecting subsurface openings.

The impulse radar profiling system produced a graphical output that displayed a close approximation to the subsurface soil, rock, water, and void interfaces. The depth of penetration was limited to a maximum of 8 ft (2.4 m) because of the presence of the moist, clay-rich soils that greatly dissipated the energy propagated by the system. An advantage of this system is that an initial version of the profile can be obtained while the survey vehicle is still in the field, which permits field personnel to auger isolated holes in order to identify the important material interfaces.

Electrical resistivity proved to be the most useful technique for delineating subsurface materials. Geoelectrical soundings are well suited to locating conductive and insulative subsurface materials. However, because of the principle of equivalence, distinguishing a water-filled cavity from another conductive subsurface layer or distinguishing an air-filled opening from another highly resistive layer may be impossible.

A combined analysis of the geophysical data provided more information than would have been available from any single system. Radar profiling and resistivity are complementary geophysical systems, and the radar system would be even more valuable if the depth of penetration under conditions encountered in the test areas could be increased. The passive microwave radiometer did not provide sufficient information to warrant its additional cost.

ACKNOWLEDGMENT

Figures 1 and 2 were provided courtesy of the State Highway Commission of Kansas.

REFERENCES

1. H. T. Rib, J. W. Spencer, C. P. Falls, and J. F. Koca. Evaluation of Aerial Remote Sensing Systems for Detecting Subsurface Cavities in Kansas. Federal

Highway Administration, FHWA-RD-75-119, 1975.
2. J. W. Spencer, J. F. Koca, H. T. Rib, and C. P. Falls. Evaluation of Geophysical Systems for Remote Sensing of Subsurface Cavities in Kansas. Federal Highway Administration, FHWA-RD-75-120, 1975.
3. Final Report on Subsurface Investigation of Mine Cavities. Geophysical Survey Systems, Inc., Billerica, Mass., 1972, 29 pp.
4. Detection and Definition of Subsurface Void Spaces by Ground-Based Microwave Radiometers. Resources Technology Corp., Houston, Texas; NTIS, PB 225 699, 1972, 150 pp.
5. L. C. Brichta and J. P. Ryan. Practical Evaluation of Electrical Resistivity Surveys as a Guide to Zinc-Lead Exploratory Drilling, Badger-Peacock Camp and Vicinity, Cherokee County, Kansas. U.S. Bureau of Mines, Rept. of Investigation 5426, 1958.
6. K. L. Cook and R. G. Van Nostrand. Interpretation of Resistivity Data Over Filled Sinks. Geophysics, Vol. 19, 1954, pp. 761-790.
7. R. G. Van Nostrand and K. L. Cook. Interpretation of Resistivity Data. U.S. Geological Survey, Professional Paper 499, 1966.
8. W. S. T. Smith and C. E. Siebenthal. Geologic Atlas of the United States. Folio 148, Joplin District, Missouri-Kansas, 1907.
9. J. R. Lundien. Terrain Analysis by Electromagnetic Means—Laboratory Measurement of Electromagnetic Propagation Constants in the 1.0 to 1.5 GHz Microwave Spectral Region. U.S. Army Engineer Waterways Experiment Station, Vicksburg, Miss., Technical Rept. 3-693, 1971.
10. R. W. Moore. An Empirical Method of Interpretation of Earth Resistivity Measurements. Transactions, American Institute of Mining and Metallurgical Engineers, Vol. 164, 1945, pp. 197-223.
11. H. M. Mooney and W. W. Wetzel. The Potentials About a Point Electrode and Apparent Resistivity Curves for a Two-, Three-, and Four-Layered Earth. Univ. of Minnesota Press, Minneapolis, 1956.
12. P. K. Bhattacharya and H. P. Patra. Direct Current Geolectric Sounding. Elsevier, Amsterdam, Netherlands, 1968.

MICROGRAVITY AND ITS APPLICATIONS TO CIVIL ENGINEERING

Gildas Omnes, Geoterrex, Ltd.

Microgravity surveys may be defined as surveys in which the accuracy of measurements is better than 0.05 mgal (0.5 $\mu m/s^2$) and the spacing between stations is less than 100 m. The development of microgravity as a tool for detecting cavities was favored because of local European conditions, particularly the numerous old underground quarries in and near the cities. A method was needed that could be used on roads still open to traffic, among or within buildings, and in gardens without causing any damage. Moreover, gravity measurements are not affected by the buried metal pipes that disturb resistivity measurements considerably. The productivity of microgravity crews was greatly increased by the introduction in 1968 of the Microgal gravity meter. Before the end of 1968, good standard gravity meters were used but stations had to be surveyed up to 3 times to obtain required accuracy. Significant anomalies of 0.020 mgal (0.2 $\mu m/s^2$) or a little less with an accuracy better than 0.004 mgal (0.04 $\mu m/s^2$) can now be studied. Microgravity has been successfully applied to the detection of several types of cavities. The amplitude of the anomaly due to a cavity frequently has been observed to be more than twice the size of the anomaly calculated on the basis of the dimensions of the cavity. A microgravity survey gives significant results only if the behavior of the gravimeter is observed continuously, the leveling of stations is carried out with an accuracy of better than 1 cm, and all calculations and corrections are adapted to the type of problem. A microgravity test carried out at Golden Hill near Boulder, Colorado, on an adit dug in a granite hill showed that the 6 by 8-ft (1.8 by 2.4-m) adit was detected at a depth greater than 20 ft (6.1 m).

•MANY European cities have been built with stone mined from underground quarries located under the cities themselves or on their outskirts. A large proportion of these quarries are centuries old and their exact location or even their existence is unknown. This also is true for old coal mines and natural cavities in limestone.

A phase of expansion for European cities began during the 1950s as larger buildings were erected, freeways were built, and the activities of the building industries were no longer restricted to the repair of damages caused by World War II. The need for a tool capable of detecting and mapping these cavities became evident. Drilling was certainly the first reconnaissance method used for that purpose. However, builders soon found out that drilling is a costly reconnaissance method. A high density of holes is necessary because the information given by a drill hole is strictly exact. A drill hole in a narrow natural dissolution joint and a drill hole intersecting a wide cavity may look the same. Working with even the lightest rigs where the land is still being cultivated or among old buildings or on roads still in use is often a problem. The advantages of a geophysical method sensitive to the volume of the cavities and based on the use of light instruments are evident.

As a consequence, the activity of Compagnie Générale de Géophysique (CGG) in the domain of cavity detection has been continual since 1958. Between 1958 and 1963, the main geophysical tool was direct-current resistivity, although some research and some tests were carried out on the application of seismic methods. Resistivity was successful enough to give rise to continual activity even though there are important drawbacks to the method. Cavities may be filled with air, mud, and rubble and give rise to resis-

tive or conductive anomalies or to no anomalies at all. Buried metal pipes disturb resistivity measurements in built-up areas. Use of even a short quadrupole array among buildings is sometimes difficult. Velocity contrasts due to cavities are generally more constant than resistivity contrasts, but the complexity of seismic sections near the surface makes the interpretation of seismic results very difficult. Electromagnetic methods are applicable where cavities are situated in very resistive rocks and where there is no clayey conductive overburden; these conditions rarely exist, at least in most temperate and tropical countries.

As early as 1940, gravimeters existed that had a sensitivity of 0.01 mgal (0.1 $\mu m/s^2$) but this sensitivity was never called on in structural studies. When the interval between stations is about 1,000 ft (304.8 m) or more, an accuracy better than 0.05 mgal (0.5 $\mu m/s^2$) is certainly not required, and gravimeters and theodolites are not used to the limits of their capabilities. Microgravity surveys may be defined as surveys where the Bouguer anomaly is defined with an accuracy better than 0.05 mgal (0.5 $\mu m/s^2$) and where the spacing between stations is less than 300 ft (91.4 m).

The first microgravity surveys were carried out on mining projects. The first paper published on the subject was by Hammer (1) in 1953 where a 0.36-mgal (3.6-$\mu m/s^2$) anomaly due to a chromite body was presented. The accuracy was estimated at 0.016 mgal (0.16 $\mu m/s^2$); the grid was 20 by 20 m. Approximately 20 years later, some surveys are carried out on a 2 by 2-m grid, and significant anomalies of 0.020 mgal (0.2 $\mu m/s^2$) or a little less are studied with an accuracy better than 0.004 mgal (0.04 $\mu m/s^2$), or 4 μgal. In 1963, Colley (2) published the first paper on the detection of caves by gravity measurements, but the topic was restricted to the detection of very large caves with a station interval of 100 m. CGG carried out its first microgravity survey for the detection of cavities in 1963 near Paris on a freeway route. Between 1963 and 1969, both resistivity and microgravity were used but the share of microgravity increased continually. Neumann (3), who supervised the development of microgravity as a tool for the detection of cavities, presented the first paper on the subject at a meeting of the European Association of Exploration Geophysicists in 1966.

There are 3 main advantages of microgravity for the detection of cavities.

1. Whether filled with air, fresh water, salt water, mud, or rubble, a cavity corresponds to a negative density contrast.
2. A gravimeter can be operated almost everywhere—on roads, on building sites, in gardens, even in basements—without disturbing the environment.
3. Gravity measurements are not affected by buried metal pipes or stray currents. Vibrations due to traffic or activity on building sites can be a problem, but operation during periods when these activities are stopped or greatly reduced is generally possible.

Until 1969, good standard gravimeters were used. An accuracy of 0.02 mgal (0.2 $\mu m/s^2$) could be obtained only by repeating measurements. Having to survey each station up to 3 times was a serious drawback. After several contacts with different manufacturers, one manufacturer came up with realistic and satisfying specifications. At the end of 1968, CGG started carrying out field work with the Microgal gravimeter. The "reading accuracy" of this gravimeter is about 2 μgal (0.02 $\mu m/s^2$), but the influence of instrumental drift is relatively stronger than for standard instruments, and the "measuring accuracy" is about 5 μgal (0.02 $\mu m/s^2$). When operated in the same conditions, the Microgal gives results affected by an error that is one-fifth of the error affecting the results obtained with a good standard gravimeter.

The introduction of the Microgal gravimeter increased the production of microgravity crews drastically. The last CGG resistivity surveys for the detection of cavities were carried out in 1971. Since 1958, 82 resistivity surveys for the detection of cavities had been carried out by CGG in Europe; among them, 8 were on freeway construction sites. Between 1963 and 1971, 55 microgravity surveys had been carried out; among them, 6 were on highways of freeway construction sites. After 1971, microgravity became the sole method used by CGG for the detection of cavities. Since the beginning of 1972, 63 microgravity surveys have been carried out for the detection of

cavities; among them, 5 took place on freeway construction sites. These figures prove that the application of microgravity to detection of cavities has been successful.

GRAVITY ANOMALIES DUE TO CAVITIES

Figures 1 and 2 show examples of theoretical anomalies corresponding to possible types of cavities. Amplitudes generally do not exceed 0.3 mgal (3 $\mu m/s^2$), and anomaly widths slightly exceed cavity widths.

After 10 years of experience with microgravity surveys over cavities, Neumann (4) said:

> The fact that measured anomalies are always larger than the anomalies calculated on the basis of the geometrical dimensions should be considered as established experimentally. Observed anomalies are frequently more than twice the size of the corresponding calculated anomalies. This is certainly a most important fact in favor of microgravity. It authorizes the application of microgravity to problems which were considered as beyond the reach of all geophysical methods a few years ago.

This phenomenon is attributed to stress relief, jointing, and dissolutions induced by the creation of the cavity. The density contrasts created by decompression, jointing, and dissolution are weak, but they affect volumes much larger and closer to the surface than the cavity itself. Figure 3 shows a weak anomaly barely larger than 0.05 mgal (0.5 $\mu m/s^2$) associated with an underground quarry. Actually this amplitude is more than twice the theoretical influence of the voids. The height of the chambers ranges between 1 and 2 m. They are 16 m deep, and the total volume of the pillars is larger than the total volume of the voids. Secondary efforts of this nature are naturally stronger above older cavities and in rocks subject to jointing and dissolution such as limestone, gypsum, and schist. They are weaker in the case of recent cavities dug in compact homogeneous rocks such as some granites or sandstones. In the case of Figure 3, it is interesting to note that the first drill holes intersected pillars. Drilling additional holes was decided on only because of the microgravity results. Contour interval in Figure 3 is 0.01 mgal (0.1 $\mu m/s^2$).

Figure 4 shows a stong anomaly due to a karstic cavity; its amplitude reaches 0.26 mgal (2.6 $\mu m/s^2$). A drill hole located at its center did not intersect any void, but refraction results showed that the limestone is replaced by loose material in locations. Subsequent geological studies showed that several karstic cavities in the area had been filled with coarse detrited material from a nearby creek. Contour interval in Figure 4 is 0.02 mgal (0.2 $\mu m/s^2$). Figure 5 shows a 0.03-mgal (0.3-$\mu m/s^2$) anomaly due to a much smaller shallow karstic cavity on a freeway building site. The small sink hole appeared after the completion of the survey when a light post was being set up. Contour interval in Figure 5 is 0.01 mgal (0.1 $\mu m/s^2$).

Figure 6 shows a fortunately rare occurrence. Anomalies A and B have almost the same amplitude. Anomaly A corresponds to a known quarry. Several drill holes on anomaly B failed to intersect any cavity. Anomaly B is now considered to be due to geological causes. Contour interval in Figure 6 is 0.02 mgal (0.2 $\mu m/s^2$).

REQUIREMENTS AND FIELD PROCEDURES

We emphasize that substituting a Microgal for a standard gravimeter is not enough. All proccdurcs should be adapted to the conditions particular to microgravity. The gravimeter operator must not be misled by the apparent simplicity of measurements. He or she must continually study the behavior of the gravimeter, temperature, and light shocks and note drift in detail. Results may be disappointing if the operator is not permanently conscious of the fact that the best possible performances are asked for. Figure 7 shows a comparison on a 2 by 2-m grid of results obtained by an operator who did not know more than taking readings (Figure 7a) with results obtained by an

Figure 1. Theoretical anomalies and detection of cavities, example 1.

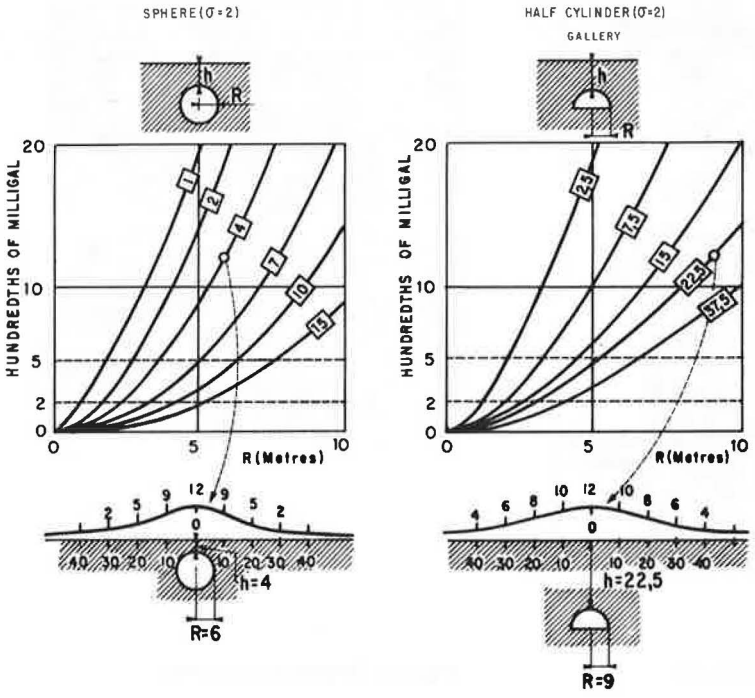

Figure 2. Theoretical anomalies and detection of cavities, example 2.

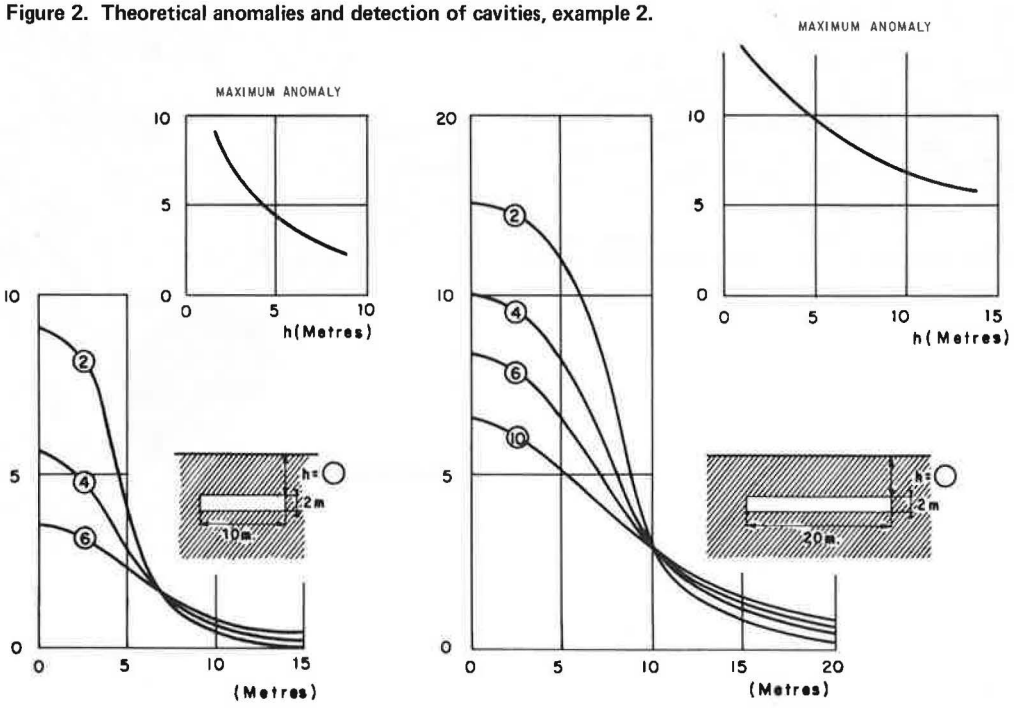

Figure 3. Residual anomaly for gravimetry and drill holes.

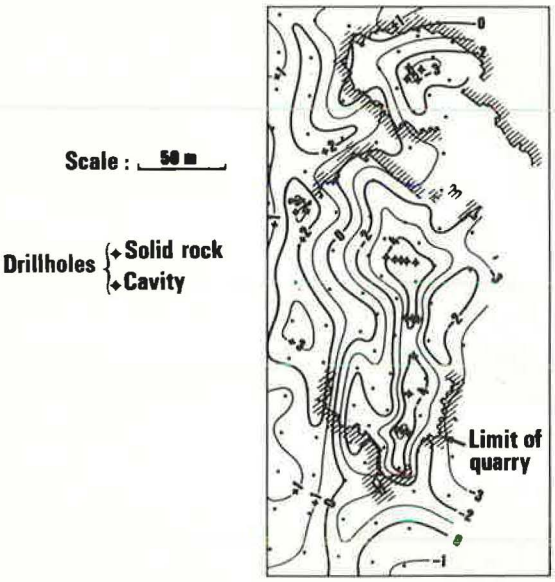

Figure 4. Detection of karstic cavities.

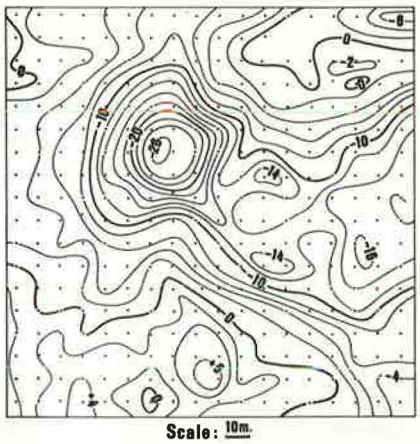

Figure 5. Detection of cavities under freeway.

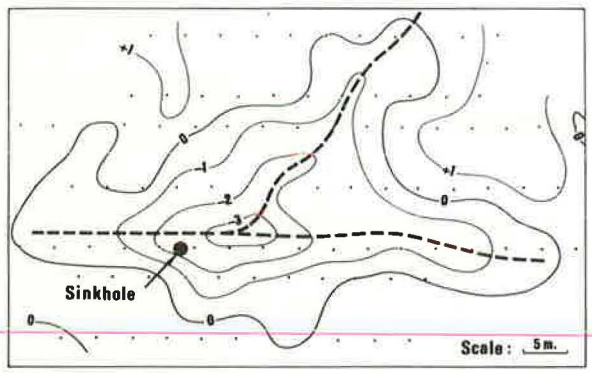

Figure 6. Detection of quarries.

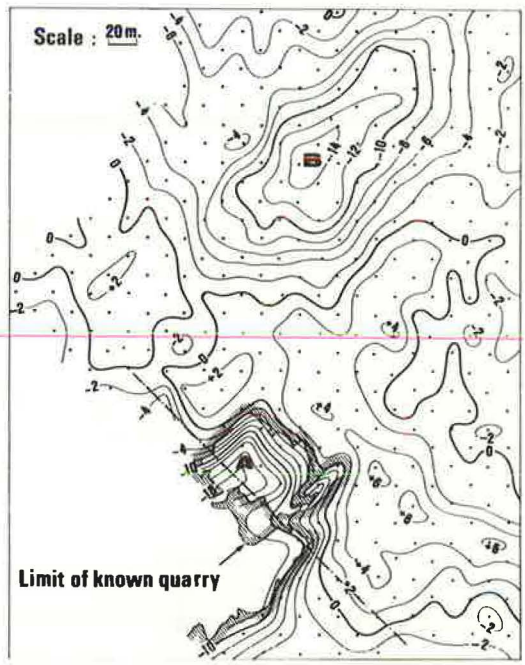

operator aware of the intricacies of the behavior of a highly sensitive gravimeter (Figure 7b).

At shallow depths the anomaly is not much wider than the anomalous body itself. Therefore, the grid should not be larger than the horizontal projection of the cavity. Figure 8 shows the result of a test over a known cavity by using 2 different grids. In Figure 8b, the exact location of the cavity cannot be deduced from the gravity anomaly.

The Bouguer anomaly may be written

$$B = g - g_0 + cz + T \qquad (1)$$

where

g = measurement in milligals (micrometers per second^2),
g_0 = value of g on the international ellipsoid in milligals (micrometers per second^2),
c = 0.3086 - (0.0419 × d) in milligals per meter (micrometers per second^2 per meter),
d = density of formations affected by elevation variations,
z = elevation in meters, and
T = terrain correction in milligals (micrometers per second^2).

The surveying should be accurate enough to render negligible the errors due to the corresponding corrections; obtaining an accuracy of 1 cm in elevation and 10 cm in position is not difficult. Terrain corrections are a more difficult problem when they are necessary. Special charts have been calculated that make use of the elevations of the surrounding stations and not of the contours. Because the extent of microgravity surveys is generally small, the effect of remote large reliefs may be considered as part of the regional anomaly. The determination of d is carried out by various methods, all of which are based on the cancellation of correlations between the variations of the Bouguer anomaly and elevation variations. Computers currently are used for this operation because the solution is sometimes complex and d varies horizontally as well as vertically.

MICROGRAVITY TEST AT GOLDEN HILL

In June 1974, a test was carried out by Geoterrex, Ltd., for the U.S. Bureau of Mines on an old adit driven in a granite hill near Boulder, Colorado. The adit is driven horizontally from the surface under a 15-deg slope. The width of the adit is approximately 6 ft (1.8 m), and its height is 8 ft (2.4 m). The adit is not located in homogeneous granite but follows shattered quartz veins.

The contoured Bouguer anomaly is presented in Figure 9. A density of 2.5 was taken for the superficial formations after other values were tested. In this case, the number of stations is too small for the application of statistical methods and the determination of variations of d.

In Figure 10, the Bouguer anomaly and a section of the ground on line 1 are plotted. A plane regional anomaly was assumed on all lines because it appears to correspond to an actual phenomenon and because the total number of stations is too small for the application of more refined calculations or a regional anomaly. Terrain corrections were not carried out because of the small size of the surveyed area located on the flank of a large hill. Terrain effects are considered as included in the regional anomaly. Figure 11 shows the resulting residual anomaly. In lines 2 and 3, a negative axis coincides with the projection of the main adit; moreover, isogals are parallel to the secondary adit.

To verify the validity of the residual anomaly, one may compare it to a map obtained through a more "objective" method. Figure 12 shows a map of an approximation of a calculated vertical gradient. This vertical gradient was calculated separately on the 3 lines by using an approximative formula reduced to the sum of 3 terms instead of the

Figure 7. Comparison of results obtained by (a) operator who did not know more than taking readings and (b) operator aware of the intricacies of gravimeter.

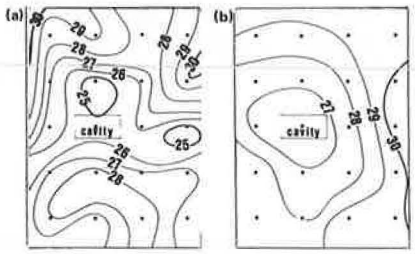

Figure 8. Importance of density of stations for (a) 2 x 2-m grid and (b) 4 by 4-m grid.

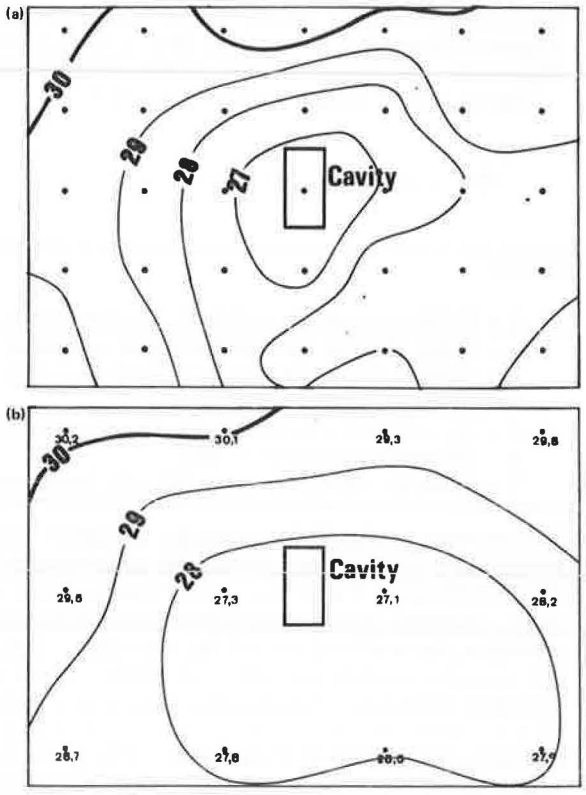

Figure 9. Golden Hill Bouguer anomaly.

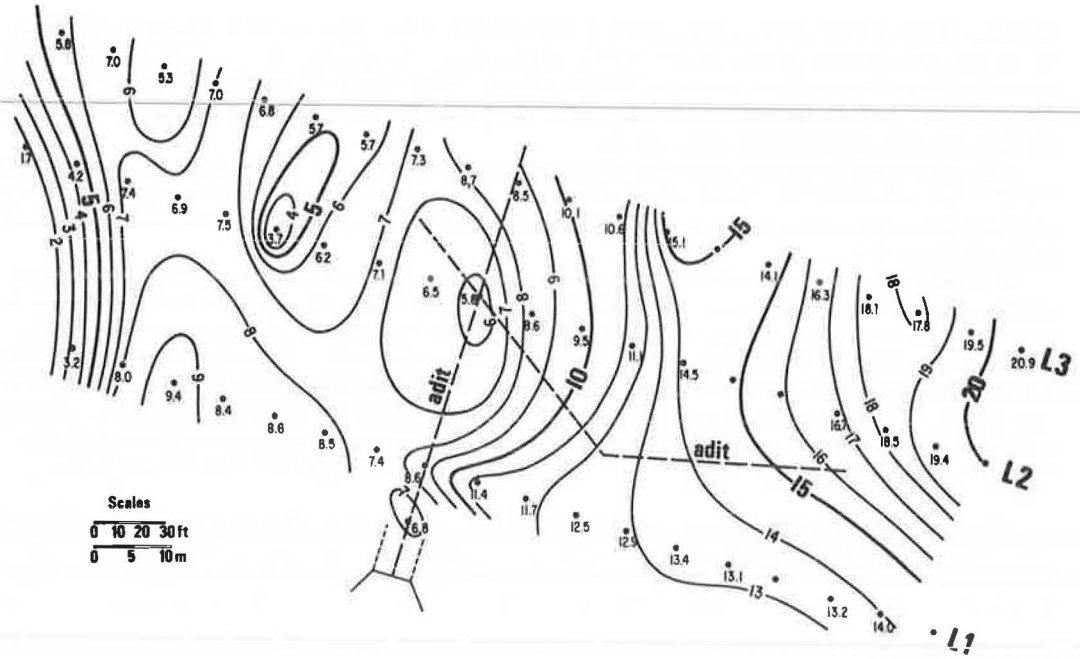

Figure 10. Golden Hill line 1.

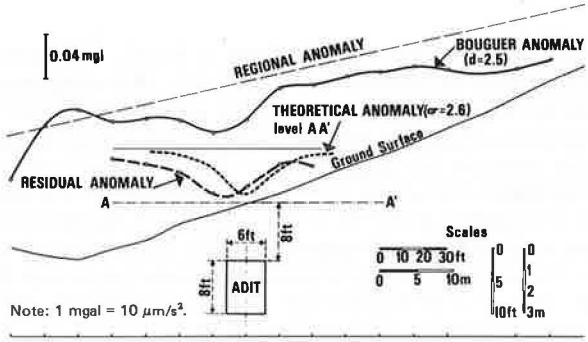

Figure 11. Golden Hill residual anomaly.

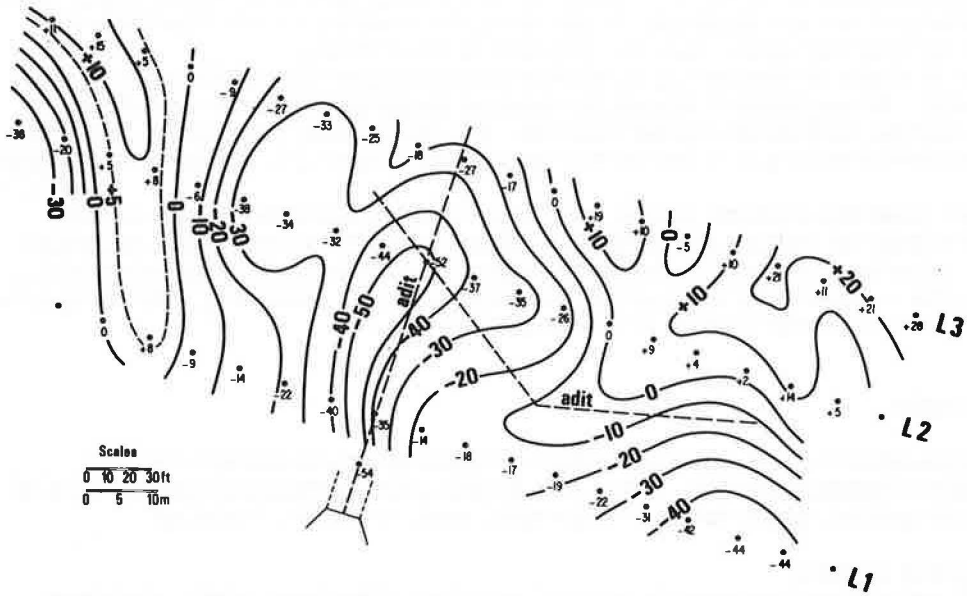

Figure 12. Golden Hill approximate calculation of vertical gradient.

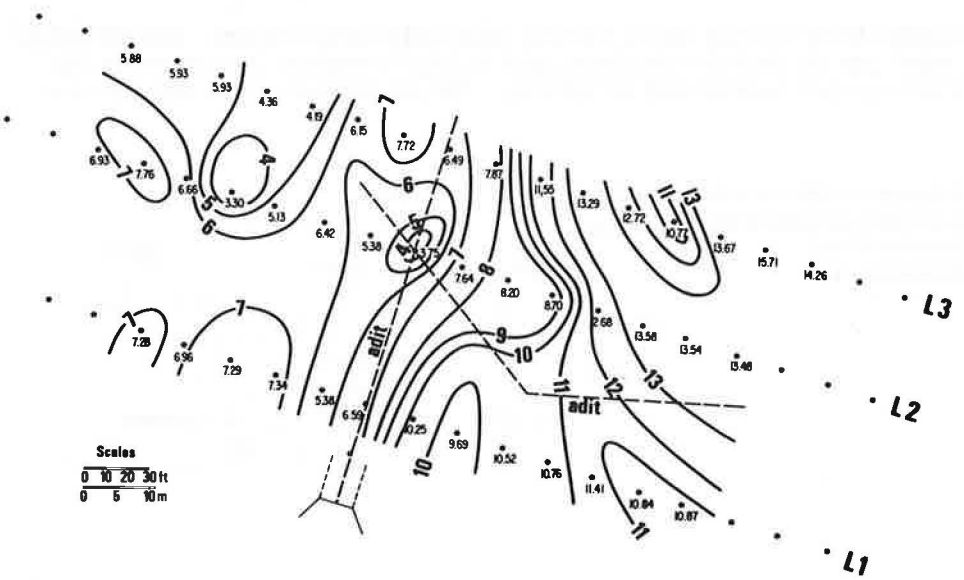

minimum of 5 generally used for calculations by hand. The result is in good agreement with the residual anomaly of Figure 11. On line 1, the minimum of the residual anomaly does not coincide with the projection of the axis of the adit (Figure 10). This could be thought to be due to a residual terrain effect similar to the effect shown in Figure 13. This effect results because the Bouguer anomaly is the difference between a measurement of the gravity field corrected for instrumental drift and lunisolar variations and a theoretical value associated with the station (5). The theoretical value is $g_0 - cz - T$. Consequently, the values of the Bouguer anomaly calculated at stations located at different elevations are affected by elevation variations as shown by Figure 13.

In some cases, the axis of an anomaly may be displaced. This effect can be compensated for by carrying out a continuation of the gravity field. A horizontal datum plane is selected, and the gravity field at the projection of each station on the datum plane is calculated. These calculations generally are carried out by computers, but an approximation can be obtained by hand. Calculation by hand is an extrapolation based on the calculated vertical gradient. In this case, the residual terrain effect was verified to be not large enough to shift the minimum of the anomaly.

Figure 10 shows the theoretical anomaly corresponding to the adit for a density contrast of -2.6. Its amplitude is almost the same as the amplitude of the experimental anomaly, and the right flanks almost coincide. The discrepancy between the left flanks can be considered to be due to low-density near-surface material, perhaps a small landslide.

Further quantitative interpretation work does not seem warranted in this case because the number of stations is relatively small and because the bedrock is not homogeneous. Also the compensation for terrain effects cannot be carried out accurately. However, the results of the test appear to be positive, and a small 6 by 8-ft (1.8 by 2.4-m) adit at a depth greater than 20 ft (6.1 m) can be detected.

CONCLUSIONS

The examples given in this paper show that microgravity is undoubtedly a well-established geophysical method. It has been particularly successful in the detection of all types of cavities, empty or filled with water, mud, or rubble, including

1. Karstic cavities;
2. Old underground quarries in various formations (limestone, chalk, sandstone, schist, and granite);
3. Old open quarries filled with rubble, soil, and the like; and
4. Old mine workings.

Most surveys were carried out on building sites and freeway routes. For historical reasons, microgravity until now has been used mainly in western Europe where the number of surveys per year is still increasing. The advantages of microgravity are

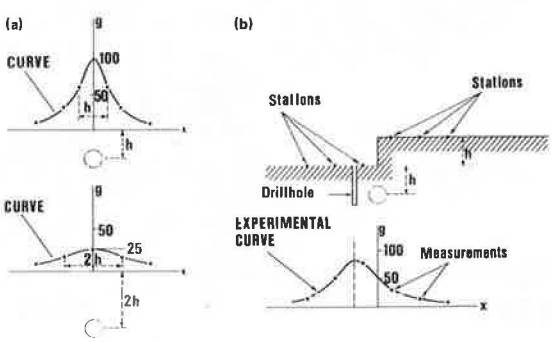

Figure 13. Influence of residual terrain effect for (a) anomalies at constant levels (upper and lower levels) and (b) experimental anomaly.

such that it can be expected to be used widely in karstic countries and in old mining areas outside western Europe.

ACKNOWLEDGMENT

I wish to thank Robert Neumann for all the documents taken from his previous papers and presented here. Figures 1 through 8 and Figure 13 are based on his work.

REFERENCES

1. S. Hammer. Usefulness of High Quality Gravity Surveys. Oil and Gas Journal, Sept. 1953.
2. G. C. Colley. The Detection of Caves by Gravity Measurements. Geophysical Prospecting, Vol. 11, No. 1, 1963.
3. R. Neumann. La gravimetrie de haute precision—Application aux recherches de cavites. Geophysical Prospecting, Vol. 15, No. 1, 1967.
4. R. Neumann. Prospection gravimetrique appliquee a la localisation des cavites souterraines. Hanover, 1973.
5. H. Naudy and R. Neumann. Sur la definition de l'Anomalie Bouguer et ses consequences pratiques. Geophysical Prospecting, Vol. 13, No. 1, 1965.
6. R. Neumann. High Accuracy Gravity—Recent Progress. Compagnie Générale de Géophysique, Paris, June 1972.

SPONSORSHIP OF THIS RECORD

GROUP 2—DESIGN AND CONSTRUCTION OF TRANSPORTATION FACILITIES
W. B. Drake, Kentucky Department of Transportation, chairman

SOIL AND ROCK PROPERTIES AND GEOLOGY SECTION
L. F. Erickson, Idaho Department of Highways, chairman

Committee on Exploration and Classification of Earth Materials
Robert L. Schuster, U.S. Geological Survey, Denver, chairman
Robert C. Deen, Edward A. Fernau, Albin D. Hirsch, William P. Hofmann, Frank L. Jagodits, Robert B. Johnson, Ralph W. Kiefer, Robert D. Krebs, Clyde N. Laughter, R. M. Mattox, Donald E. McCormack, Olin W. Mintzer, R. Woodward Moore, Arnold C. Orvedal, David L. Royster, A. Rutka, Robert B. Sennett, William W. Shisler, Preston C. Smith, Ernest G. Stoeckeler, J. Allan Tice, Walter H. Zimpfer

John W. Guinnee, Transportation Research Board staff

The organizational units and the chairmen and members are as of December 31, 1974.